Lognormal firing rate distribution reveals prominent fluctuation–driven regime in spinal motor networks

Peter C. Petersen[1] ***and Rune W. Berg***[1]*

[1] *Faculty of Health and Medical Sciences, Department of Neuroscience and Pharmacology, University of Copenhagen, Blegdamsvej 3, 24.3.47, DK-2200 Copenhagen N, Denmark*

∗*Correspondence: runeb@sund.ku.dk*

ABSTRACT

When spinal circuits generate rhythmic movements it is important that the neuronal activity remains within stable bounds to avoid saturation and to preserve responsiveness. In what dynamical regime does the neuronal population operate in order to achieve this? Here, we simultaneously recorded from hundreds of neurons in lumbar spinal circuits and establish the neuronal fraction that operates within either a 'mean-driven' or a 'fluctuation–driven' regime during generation of multiple motor behaviors. We find a rich diversity of firing rates across the neuronal population as reflected in a lognormal distribution and demonstrate that half of the neurons spend at least 50% of the time in the 'fluctuation–driven' regime regardless of behavior. Since neurons in this regime have a 'supralinear' input–output curve, which enhances sensitivity, whereas the mean–driven regime reduces sensitivity, this fraction may reflect a fine trade–off between stability and sensitivity in order to maintain flexibility across motor behaviors.

INTRODUCTION

During sensory and motor processing, neural circuits must be able to retain sensitivity and perform operations, while maintaining stability to avoid run–away excitation [Vogels *et al.*, 2005]. How networks, especially spinal networks, manage to maintain in stable states in between unresponsive quiescence and saturation is an open question. Stability has primarily been investigated in sensory networks in the neocortex from a theoretical perspective, but the issue is important for any circuit in the central nervous system. Inhibition is a core component of generation of movements [Britz *et al.*, 2015] and feedback inhibition is a key mechanism in stabilizing the dynamics of neuronal circuits [Hansel and Mato, 2001; Ikegaya *et al.*, 2013], which may indicate a purpose of the omnipresent *balanced excitation (E) and inhibition (I)* [Amit and Brunel, 1997; Berg *et al.*, 2007; Kumar *et al.*, 2008; Okun and Lampl, 2009; Ozeki *et al.*, 2009; van Vreeswijk and Sompolinsky, 1998]. The stability of neuronal networks is also associated with the shape of the input–output (IO) function of neurons. An IO–function in which the response to multiple inputs is larger than the sum of their individual responses (i.e. *supralinear*) will tend to enhance sensitivity and amplify fluctuations from recurrent excitation [Rubin *et al.*, 2015]. This is in contrast to a *sublinear* summation, which will curb activity while the combination of these two functions into a sigmoidal shape may explain a wide variety of circuit properties [Ahmadian *et al.*, 2013]. Interestingly, neurons receiving fluctuating synaptic input have S-shaped IO-curves [Silver, 2010], where the left part below threshold (rheobase) consists of an upward concave curvature akin to a power–law where the spikes are driven by transients [Miller and Troyer, 2002; Priebe and Ferster, 2005; Vestergaard and Berg, 2015], and the right part above threshold is linear or even sublinear (**Figure 1**). Spikes evoked

Table 1: Two regimes of neuronal spiking and their definition, properties and causes.

	Fluctuation–driven	**Mean–driven**	**Key references**
Definition	$R_m I_{total} < V_{thres}$	$R_m I_{total} > V_{thres}$	[Brunel, 2000; Gerstner *et al.*, 2014]
Properties	Lower firing rates	Higher firing rates	
	Irregular spiking	Regular spiking	[Amit and Brunel, 1997] [Shadlen and Newsome, 1998] [van Vreeswijk and Sompolinsky, 1998]
	Skewed distribution	Symmetric distribution	[Buzsáki and Mizuseki, 2014] [Mizuseki and Buzsáki, 2013; Roxin *et al.*, 2011]
Cause	Balanced E/I Synchronized excitation	Intrinsic currents, unbalanced E/I	[Shadlen and Newsome, 1994] [Softky and Koch, 1993] [Stevens and Zador, 1998]

by synaptic transients belong to the *fluctuation–driven regime* [Kuhn *et al.*, 2004; Tiesinga *et al.*, 2000], which is in contrast to *mean–driven* spikes where the mean membrane potential (V_m) is well above threshold [Gerstner *et al.*, 2014; Renart *et al.*, 2007]. These two regimes have contrasting manifestations (Table 1): the fluctuation–driven regime has irregular spiking and a skewed output whereas the mean–driven regime has regular spiking and a symmetric firing rate distribution (**Figure 1a–c**). The degree to which neurons within a population operate in one versus the other regime may hold the key to understanding stability, dynamic range and other important properties of network operations.

Here, we investigate the regimes of operation of spinal neurons during different rhythmic motor behaviors, which are generated in the lumbar spinal circuits of turtles. The mechanical stability of the turtle preparation allows electrophysiological recordings of unprecedented quality, and the high resistance to anoxia of turtles allows using adult animals with fully developed spinal circuitry, which have healthy network activity and which can perform multiple complex motor behaviors [Stein, 2005]. We use distinct scratch reflexes to investigate the population activity during multiple motor behaviors. The population consists of both motoneurons and spinal interneurons, which were widely sampled in order to cover as many cell types as possible and capture network activity. The custom designed high–density silicon electrodes recorded the population activity from hundreds of cells in the dorso–ventral and rostro–caudal axes along with the intracellular V_m of single neurons and multiple relevant motor nerves (**Figure 2**).

Our experiments demonstrate the presence of both regimes with a rich diversity of occupation across the neuronal population. The distribution of synaptic input to neurons in the fluctuation–driven regime had a symmetric Gaussian shape, which suggest that the skewness in the firing rate output is due to the nonlinear transformation rather than a linear transformation of a skewed input distribution (**Figure 1**). This subthreshold response function has a nonlinear shape akin to a power–law function. This is in qualitative agreement with the theoretical scheme put forward by Roxin *et al.* [2011]. Next, we assessed the firing rate distribution across the population in parallel with the irregularity in order to establish the fraction of neurons, which are either in the fluctuation– or mean–driven regime in time and across behaviors. We found half of the neurons spend at least 50% of their time in the fluctuation–driven regime. Since this fraction is preserved across behaviors as well as animals, it may represent a fundamental trade–off between sensitivity and stability in the range of operation of spinal motor networks.

RESULTS

Neuronal spiking has traditionally been considered to occur when the mean inward current of the cellular membrane is large enough to cross the rheobase such that the mean membrane potential (V_m) is above threshold (V_{thres}). In practice, the mean V_m will not exceed V_{thres} by very much due to the active spikingand after–hyperpolarization, but if this mechanism was turned off the mean membrane current (I_m) would drive V_m across threshold, formally written as $I_m > V_{thres}/R_m$ where R_m is the membrane resistance. Spikes elicited in this manner are in the *mean–driven* regime [Gerstner *et al.*, 2014; Renart *et al.*, 2007]. They have shorter inter–spike intervals (ISIs) because of the large I_m and regular spiking due to the after–hyperpolarization. In contrast, when the mean V_m is below threshold, i.e. $I_m < V_{thres}/R_m$ and spikes are elicited by temporary fluctuations in V_m due to synaptic bombardment. Such spiking is in the *fluctuation–driven* regime [Gerstner

et al., 2014; Kuhn *et al.*, 2004; Roxin *et al.*, 2011; Tiesinga *et al.*, 2000]. The random synaptic fluctuations causes the spiking to be more irregular, which results in a higher coefficient of variation (CV, defined as the standard deviation (σ) divided by the mean of ISIs), than for the mean–driven regime (cf. **Figure 1D–E**). Therefore irregularity is a indicator of which regimes the spiking belongs to. Another indicator of the fluctuation–driven regime is positive skewness of the firing rate distribution (**Figure 1A-B**). We will use these indicators to quantify the fraction of the population that is in one regime versus the other.

We use the spinal circuitry of the adult turtle, to address the participation of neurons in the two regimes during motor activity across a neuronal population. The turtles high anoxia tolerance, allow us to use adult animals to investigate multiple and very complex motor behaviors, while getting stable highquality electrophysiological recordings. The parallel spiking activity of about 200 single units were recorded with multi-channel arrays, which were inserted into the ventral horns of lumbar spinal segments (**Figure 2A**) to record spinal neurons involved in motor rhythm generation. The location of the electrode arrays in the ventral area of the lumbar enlargement was verified by histology (**Figure 2B-C** and **Figure supplement 1**). The array recordings were performed simultaneously with recording of the intracellular activity of a single neuron in parallel with electroneurograms (ENGs) from relevant motor nerves (**Figure 2D**). Site–specific rhythmic hindlimb scratching was induced by tactile touch of the carapace [Berkowitz *et al.*, 2010; Stein, 2005] and could be reproduced reliably over multiple trials [Petersen *et al.*, 2014; Vestergaard and Berg, 2015]. Extracellular multielectrode arrays, which were custom–designed for the spinal cord (Berg64-probe, Neuronexus inc.), enabled simultaneous recording from and spike sorting of 200-300 single units, which remained stable over many trials (**Figure 2e** and **Figure supplement 2**). The distribution of firing rates across the population had a positive skewness on a linear scale and near zero skewness on a log scale (**Figure 2F**), which indicates a wide degree of participation in the motor activity across the population.

Gaussian input and skewed output

To verify the presence of both spiking regimes, we first look at serially acquired intracellular recordings. We do not consider the time where the neuron is not spiking in a burst cycle, i.e. when they are in *off–cycles* between bursts (**Figure 1D–E**), and thus ignore periods, where V_m is far from V_{thres} and in an irrelevant part of the IO–function. To quantify the output, we start with the distribution of the instantaneous firing rates, i.e. the inverse of ISIs. The majority of the cells were positively skewed on a linear-scale and normaldistributed with near zero skewness on a log-scale (**Figure 3A**). This is expected for poisson–like spiking in the fluctuation–regime [Ostojic, 2011]. Nevertheless, distributions for all the intracellularly recorded neurons ($n = 68$) were skewed to a varying degree from strong positive on a linear axis (and zero on the log–axis) to zero skewness on a linear axis (and strong negative on log–axis) (**Figure 3B**). This suggest that neurons are found in a spectrum between fluctuation– and mean–driven spiking. Neurons that have more negative log–skewness are also spiking at higher mean rates (**Figure 3C**) as expected for the mean–driven spiking, where the rate distribution is more symmetric on a linear axis with higher mean rates (Table 1).

Two alternative models have been proposed to describe the mechanism involved in lognormal firing rate distribution. The distribution could arise from a nonlinear transformation of normally distributed inputs or a linear transformation of lognormally distributed synaptic inputs [Roxin *et al.*, 2011] or a linear transformation of a lognormally distributed synaptic input [Wohrer *et al.*, 2013]. The latter mechanism has been considered in connection with the sparse spiking activity in auditory cortex [Hromádka *et al.*, 2008; Koulakov *et al.*, 2009] and since synaptic weights within neocortex have a heavy tail lognormal distribution rather than a Gaussian distribution [Ikegaya *et al.*, 2013; Song *et al.*, 2005]. Models also show that the V_m distribution is skewed but approaches a Gaussian when the rate of synaptic input increases [Ostojic, 2011]. Therefore it is important to assess whether the synaptic current is normally distributed as suggested in the *diffusion limit* of models [Richardson and Gerstner, 2006] or lognormally distributed as an alternative. We estimated the synaptic input during the peak of a locomotor cycle where the V_m is within realm of V_{thres} (**Figs. 1D** and **3D**). The synaptic current is difficult to assess, but we can approximate its fluctuations via the fluctuation in V_m under the following conditions. Between spiking, the mean V_m is just below threshold and does not change its value much. Therefore the voltage–activated conductances are approximately constant such that there should be an Ohmic relationship between synaptic current and V_m. This is justified for neurons in fluctuation–regime, since the conductance is often high, rapid and dominated by balanced synaptic input [Destexhe *et al.*, 2003; Kumar *et al.*, 2008], and thus the coupling between V_m and intrinsic conductance is suppressed in a divisive

manner [Kolind *et al.*, 2012; Tiesinga *et al.*, 2000]. We therefore selected neurons using a novel metric, *the return map ratio*, which were primarily in the fluctuation–regime (**Figure 3 supplement 1**). The return map ratio quantifies fluctuation in the subthreshold V_m between spikes and forms the basis for selecting neurons (if metric < 0.7). A sample neuron in the fluctuation–regime (**Figure 3D–E**) illustrates how we obtain the distribution of sub–threshold V_m and how we estimate the IO-curve. The distribution is estimated both by selecting the V_m in between spikes (temporal distribution) and by collecting instances of V_m prior to spike peak in a spike triggered overlay ('sigma' in **Figure 3E**). The two estimates are in agreement with one another for the sample cell (**Figure 3F**). This agreement is also found across the population as quantified by the mean and SD (**Figure 3G**). The skewness is small and scattered around zero (**Figure 3 supplement 2A inset and 3**) as expected for normally distributed current input. From these data we conclude that the input distribution to neurons is not skewed, but rather symmetrical and *Gaussian–like*, which is the minimal requirement for confirming the two–regime hypothesis for the single neuron (**Figure 1**). The second requirement is an IO–curve nonlinearity, which can transform the normally distributed input to a lognormal output for single neurons. To test this, it is necessary to estimate the IO–curve for subthreshold spiking.

Estimating subthreshold neuronal response–function.

We investigate the input–output function in the subthreshold region to probe its nonlinearity. Since the IO function of neurons is a fundamental property of the nervous system, it is well-characterized both theoretically [Gerstner *et al.*, 2014] and experimentally [Silver, 2010]. Here, we estimate the IO-function for sub–threshold spiking via the probability of eliciting a spike as a function of V_m in the following way. First, we collected instances of V_m shortly before the spike–onset, where V_m is depolarized yet still not part of the deterministic spike trajectory. The probability that a given value of V_m will result in a spike is estimated as the histogram of V_m–instances (green histogram, **Figure 3E**) divided by the total time spent at all values of V_m (gray histogram). This gives the dependence of the firing rate on V_m [Jahn *et al.*, 2011; Vestergaard and Berg, 2015], and it is approximately the relationship between firing rate output and the synaptic current input, using V_m as a qualitative proxy for current. This neuronal response function had a strong non–linear shape (**Figure 3H**). To capture the curvature we fitted both a power–law and an exponential and the curvature had a weak negative correlation with the SD of the V_m–fluctuation (**Figure 3 supplement 2**) as demonstrated previously [Vestergaard and Berg, 2015]. Similar expansive nonlinearity has previously been characterized in sensory–driven neurons [Anderson *et al.*, 2000; Hansel and van Vreeswijk, 2002; Miller and Troyer, 2002]. In spinal networks the non–linearity is likely involved in optimizing motor control [Vestergaard and Berg, 2015] and will transform the normally–distributed synaptic input into a *log–normally*–distributed (skewed) spiking output (**Figure 1A**). For mean–driven spiking the IO-curve is not supralinear, but rather linear (or even sublinear), and the normally–distributed synaptic input will therefore be transformed to a normally distributed spiking output (**Figure 1B**). We do not know whether the synaptic input is also normally distributed in the mean–regime, but since the synaptic input is normally–distributed in the subthreshold region (**Figure 3F**), it is likely also normally–distributed in the suprathreshold region. Otherwise, the input statistics of the presynaptic neurons would have to depend on its threshold, which is implausible. In conclusion, the skewness of the firing rate distribution is an indication of which regime the spiking belongs to.

Time spent in regimes: intracellular data

A given neuron is not likely to be just spiking in either the fluctuation– or the mean–driven regime, rather, it likely spends time in both regimes during motor activity. To estimate the amount of time a given neuron spends in either of the two regimes we calculate the fraction of time that the smoothed V_m is above versus below threshold. An example neuron, which spends most of the time below threshold (**Figure 4A**), has more irregular spiking as quantified by a local measure of irregularity, the CV_2 (green line). CV_2 is the difference of two adjacent ISIs divided by their mean [Bruno *et al.*, 2015; Holt *et al.*, 1996]. Another sample neuron that spends most time above threshold has more regular spiking, i.e. CV_2 closer to zero (**Figure 4B**). Since the threshold is firing rate–dependent (**Figure 4 supplement 1**) we use the initial threshold value (broken line), which is not distorted by inactivation of the Na^+–conductance. The distribution CV_2 for all trials has higher mean for the fluctuation–driven cell than the mean–driven (arrows, **Figure 4C**). Also, the cumulative time spent below threshold is higher for the fluctuation–driven cell (96%) than the mean–driven cell (35%,

Figure 4D). This fraction of time spent below threshold is quantified for the whole population of neurons ($n = 68$) and the distribution had a strong mode at 1 (top, **Figure 4E**). To compress the diversity within the population into a simpler representation, we use the reverse cumulative distribution of neurons versus time spent below threshold (bottom, **Figure 4E**). This indicates how many neurons (y-axis) spend at least a given fraction of time (x-axis) below threshold. The intercept with the 50%–line (broken line) indicates what fraction of time half the population at least spend below threshold. This fraction is remarkably high (84%) suggesting that the fluctuation–regime predominates.

Blocking inhibition causes change in regime

An alternative to injecting electrode current is to manipulate the balance of excitation and inhibition (E/I) by pharmacological means. We manipulated the synaptic input in a reduced preparation with a micro–superfusion of strychnine, a glycinergic blocker, over the transverse cut surface of the spinal cord (described in [Berg *et al.*, 2007; Vestergaard and Berg, 2015]), which affects neurons at the surface ($<300\mu$m) without affecting the rest of the network, which was verified by monitoring flow and the network activity via the nerve recordings. Comparing the spiking during control condition (**Figure 5G**) with that during blockade of inhibition (**Figure 5H**). Reducing glycinergic inhibition with strychnine tips the balance of E/I toward larger inward synaptic current, which results in higher firing rates, lower irregularity (green line) and a mean V_m (blue line) well above threshold (arrows, **Figure 5G–H**). The distribution of CV_2 was higher in the control than in the unbalanced case (**Figure 5I**) similar to the results observed with current injection (**Figure 5A–D**). The irregularity is also negatively correlated with depolarization of the mean V_m when unbalancing the E/I although it is uncorrelated in the control condition, where the spiking is in the fluctuation–driven regime (**Figure 5 supplement 1**). The instantaneous firing rate is skewed and log–normally distributed in the control case (top, **Figure 5J**), similar to the above sample cell (top, **Figure 5E**). When unbalancing the synaptic input, the firing rate increases (compare broken lines, **Figure 5J**) and the distribution becomes negatively skewed (compare -0.2 and -1.5) as expected in the mean–driven regime (bottom, **Figure 5J**). Similar to the analysis performed in the previous section (**Figure 4D**), the cumulative time spent below threshold is larger in the control condition compared with when inhibition is blocked (**Figure 5I**). This is consistent with a depolarization due to disinhibition, thus 'unbalancing' the excitatory and inhibitory input. These observations are also consistent with the consensus view that irregular fluctuation–driven spiking is likely due to concurrent excitatory and inhibitory synaptic input (Table 1).

Rich diversity in population firing rates

So far the analysis has been performed on serially acquired intracellular recordings across trials and animals. This demonstrates that some neurons spikes primarily in the fluctuation–driven regime while others in the mean–driven regime. Nevertheless, it is still unclear what the parallel population activity is during a behavior and across behaviors. How many neurons are in one versus the other regime and for how long? First, we assess the neuronal participation in the motor patterns by their degree of spiking, during motor behavior. Neurons were active during both ipsi– and contralateral scratching behaviors (**Figure 6A–D**). Most units had a rhythmic relationship with the nerve signals and a higher firing rate for the ipsilateral scratching compared with contralateral scratching behavior (cf. **Figure 6C** and **D**; Movie supplement 1 and 2), which indicates participation of the contralateral movement to a lesser degree than the ipsilateral movement.

The distribution of firing rates across the neuronal population over several trials (a single trial is typically 10-15 seconds long, $n = 14$) is strongly skewed, which indicate that most neurons spikes relatively infrequently with a 'fat-tail' of higher spiking (**Figure 6E**). The distribution covers two orders of magnitudes from 0.1–10Hz and is akin to a lognormal distribution (inset and green lines, **Figure 6E**). Similar lognormal–like distributions have been observed in other parts of the nervous system [Buzsáki and Mizuseki, 2014]. The implication of the skewed distribution is that most neurons spike at low rates, but there are relatively many neurons spiking at higher rates indicating a rich diversity of neurons in both the fluctuation–driven and mean–driven spiking regimes.

Mean V_m across the population is normally distributed

The foundation of the skewness in population rate distribution is not necessarily directly linked to the skewness of the instantaneous rate distribution of single neurons. The analysis of single neuron recordings show that many but not all neurons have a skewed lognormal-like firing rate distribution. This is dependent on whether they spike at a high or low rate (**Figure 3A–C**). Nevertheless, evidence suggest that the same mechanism is behind the population rate skewness as is behind the firing rate skewness of individual neurons. Not only is the subthreshold V_m normally distributed (**Figs. 3F** and **supplement A**); so is the distribution of mean V_m across neurons (**Figure 3G**, top). Nevertheless, since the spike threshold may differ between neurons, the distribution of mean V_m with respect to the nonlinear IO-curve is more critical. Therefore it is more important to know the distribution of mean V_m from threshold with respect to the size of synaptic fluctuations, i.e. standard deviation of V_m (σ). This distribution, i.e. $(V_m - V_{thres})/\sigma$, turns out to also be normally distributed with a mean around 3σ from threshold (**Figure 3 supplement 3**). If we assume, when normalizing V_m this way, the the IO-curve has approximately the same nonlinearity across all neurons (**Figure 3H**), the population distribution of firing rates will also be skewed due to the nonlinear transformation of the normally–distributed input (**Figure 3 supplement 3f**) to a lognormally–distributed output (**Figure 1a**). These results are in qualitative accordance with the scheme proposed by [Roxin *et al.*, 2011]. Thus, the skewness in population firing rates is an indicator of the degree of participation in the fluctuation–driven regime.

Skewness preserved across behaviors

Though multi–functional spinal units have been observed previously [Berkowitz *et al.*, 2010] it is unclear how their participation is distributed and whether the asymmetry in distribution is linked to different behaviors. To address this issue we analyze the population spiking for multiple motor behaviors. The induction of a distinct scratch behavior is location–specific [Stein, 2005]. Multiple behaviors can be evoked depending on exact location and which side of the body is touched. This allowed us to induce two distinct behaviors: ipsi– and contralateral hindlimb scratching, while recording from the same neuronal ensemble (**Movie supplement 1** and **2**), and these behaviors were reproducible over multiple trials (>9 trials). Both behaviors had similar phase relationships between the muscle synergists, although ipsilateral scratching had stronger activity (cf. **Figs. 6A** and **B**). The firing rate distribution was positively skewed in both behaviors with the similar qualitative shape (**Figure 6E-F**). These two behaviors were characterized across animals as well ($n = 5$) and their positive skewness in firing rate distribution remained large and positive (green bars, **Figure 6G**) and close to zero on log–scale, i.e. lognormal (black lower bars). To further quantify the uneven neuronal participation we use Lorenz statistics and the *Gini-coefficient* [Ikegaya *et al.*, 2013; O'Connor *et al.*, 2010]. The Lorenz curve characterizes the share of cumulative participation of individual neurons of the population (**Figure 6H**). The diagonal corresponds to the case where all neurons have the same firing rate. The deviation from equality is quantified by the Gini–coefficient, which is the fraction of area a to the total area $a + b$ (**Figure 6H**). The higher the coefficient, the more unequal the participation across neurons is. Both scratch behaviors had a Gini–coefficient of $\sim$0.5 (**Figure 6I**), though the ipsilateral behavior had a higher Gini coefficient (greater inequality). Though the mean firing rate can change between behaviors and between animals (**Figure 6J**), the skewness remained qualitatively preserved across behaviors (**Figure 6K**). This suggests that the skewed lognormal–like firing rate distribution, and hence a presence of the fluctuation–driven regime, is a widespread property of spinal motor networks.

Prominent occupancy of the fluctuation regime across population and time

Neurons do not occupy either the fluctuation– or the mean– driven regime all the time. Individual neurons can move back and forth between regimes depending on the synaptic current they receive. How much time does a given neuron spend in each regime? To address this, we analyze the spiking across neurons in parallel. First, we estimated the time–dependent firing rate of each neuron in the population using optimal Gaussian kernel [Shimazaki and Shinomoto, 2010] and measure skewness of the population distribution. The time–dependent population distribution was achieved by binning the rates in 10 ms windows. The mean population rate and its SD are indicated as white $\pm$ gray lines (**Figure 7A**). As the rate is increasing the skewness of the distribution plotted on a log–scale is becoming negative as a sign of more neurons occupying the mean–driven

regime (compare inset histograms, **Figure 7A**). This is further confirmed by a negative correlation between the mean population rate and the log–skewness for all time points (**Figure 7B**). To further gauge the division of neurons in the two regimes we compared the irregularity of the spiking. The distribution of the mean CV_2 across the population of neurons is clustered around 1 if all ISIs are included (gray histogram, **Figure 7C**). However, measuring the irregularity in the motor cycles alone i.e. excluding the inter–burst intervals the mean irregularity across neurons is lower and clustered around 0.6 (red histogram). Both distributions have substantial spread around the mean, which is an indication of a rich diversity spiking patterns and occupation of regimes.

To get a compound measure of the behavior of the entire population across time, we consider the amount of time each neuron spends in the fluctuation–regime. We demarcate the fluctuation–regime as having irregularity in spiking above a critical value, i.e. $CV_2 > i_{crit}$. Choosing i_{crit} is not entirely objective. Complete Poisson–type irregularity has $CV_2 = 1$, but the spiking is still irregular for lower values. Based on our data, even when the $CV_2 \approx 0.5$, the V_m spends as much as 95% below threshold (**Figure 4C–D**) indicating the fluctuation–regime. Further, neurons that have $CV_2 \approx 0.5$, also have lognormal firing rate distributions (**Figure 5**), which also indicates the fluctuation–regime. For these reasons, we suggest choosing $i_{crit} = 0.5$ for distinguishing regular vs. irregular spiking, which is also consistent with the distinction between regular vs. irregular 'choppers' in the cochlear nucleus [Young *et al.*, 1988], though they use the CV–metric. Thus, the population of spinal neurons had a large diversity in time spent in the fluctuation–regime. Some neurons spend as little as 20% in the fluctuation–regime while other spend as much as 80%. To get a quantitative handle on the occupation of neurons in the fluctuation–regime across the population, we consider the distribution of time spent with $CV_2 > i_{crit}$. This is formally quantified using the reverse cumulative distribution of neurons that spend a given fraction of time in the fluctuation–regime (**Figure 7D**). The reverse cumulative distribution is plotted for 3 values of i_{crit} (0.4, 0.5 and 0.6) to indicate the sensitivity to parameter choice. Obviously, choosing a lower i_{crit} results in a given fraction of the population spend more time in the fluctuation–regime, i.e. the curve is shifted to the right. Choosing i_{crit} larger has the opposite effect. This inverted S–shaped curve gives the fraction of neurons (y–axis), which spends at least a given time in the fluctuation regime normalized to 100% (x–axis). Hence, half of the population spent at least 58% of time in the fluctuation regime during ipsilateral scratching (intercept of curve with the broken line, **Figure 7D**). We refer to this metric as the *time in the fluctuation–regime for half the neurons* (TIF_{50}). Similar TIF_{50}–values were obtained for all five animals (inset histogram). Qualitatively similar results were achieved for a different motor behavior, namely contralateral scratching (**Figure 7E**). The TIF_{50} metric is a time–weighted analysis of irregularity of spike trains. In addition to measuring the time in regimes, we measure how many spikes are in one regime vs. the other. Hence, we calculate the reverse cumulative distribution of neurons that are in the fluctuation–regime (**Figure 7 supplement 1**). Similar to TIF_{50}, we define a spike–weighted metric as the *spikes in fluctuation regime for half the neurons* (SIF_{50}). Both the SIF_{50}– TIF_{50}–values are relatively conserved across animals as well as behaviors (**Figure 7D–E**, **supplement 1**). The large values of TIF_{50} and SIF_{50} indicate that the fluctuation–regime has a strong presence during motor behaviors, and the high similarity suggests that it may represent a conserved fundamental property of network activity.

DISCUSSION

In neuronal networks, spikes are generated in either in the *mean–* or the *fluctuation–driven regime* [Brunel, 2000; Gerstner *et al.*, 2014; Kuhn *et al.*, 2004; Tiesinga *et al.*, 2000]. In this report we present evidence for the existence of both regimes during motor pattern generation in the spinal cord. We consistently find normally distributed synaptic input combined with the supralinear shape of the IO–function in the subthreshold region, and suggest this as a compelling mechanism behind the lognormal population firing rate distribution [Roxin *et al.*, 2011]. Using spiking irregularity across the neuronal population as a hallmark of the fluctuation regime, we find that half of the neurons spend at least 50% of the time in this regime. Thus, the fluctuation–regime is not a rarity, but rather has a prominent presence both across behaviors and across animals (**Figure 7**). To our knowledge this is the first report, which quantifies occupation within spiking regimes of a neuronal population, not just in the spinal cord, but also in the nervous system in general.

Stability and the two regimes

The fact that the relative time during which a subset of neurons occupies one of the two regimes is conserved across both behaviors and animals could indicate a key principle of neuronal processing. A fundamental challenge for neuronal networks is to perform functions while keeping the population activity from falling into either of the two extreme states: 1) the quiescent state where the neuronal spiking activity cannot remain self–sustained and 2) the unstable state of run–away recurrent spiking activity [Kumar *et al.*, 2008; Vogels *et al.*, 2005]. It is well known that recurrent inhibition is important for maintaining stability, but other mechanisms may participate as well, e.g. synaptic depression or active adjustment of the shape of the neuronal response function. A nonlinear response function, as we observed in the fluctuation–regime (**Figure 3H**), will amplify input via supralinear summation [Rubin *et al.*, 2015]. The upward curvature will enhance synaptic fluctuations, which then accelerates the recurrent excitatory activity causing an unstable runaway state. In contrast, the response function in the mean–driven regime, is linear or even sublinear, which is likely to curb strong input. We therefore propose that the close proximity of the TIF_{50}–value to 50% is an indication of a self–organizing trade–off between sensitivity and stability in order to preserve at once both network homeostasis and dynamical functionality. This conjecture remains to be further substantiated in future studies. Furthermore, the TIF_{50}– and SIF_{50}–values remain to be determined for other part of the nervous system and in other species.

Rhythm generation and regimes

The distinction between fluctuation– and mean–driven spiking is interesting because the two types of spiking may have radically different causes, and this may hold an important clue to understanding the enigmatic motor rhythm generation. The fluctuation–driven spiking is believed to be caused by concurrent and random arrival of excitatory and inhibitory potentials resulting in a fluctuating subthreshold V_m (**Table 1**). In the mean–driven regime, on the other hand, the net membrane current is so large that the mean $V_m \pm \sigma$ is above threshold, and the ISIs are therefore determined by the recharging of the membrane capacitor following the refractory period of the previous spike [Powers and Binder, 2000]. This results in a deterministic trajectory of V_m and regular ISIs. More importantly, for the mean–driven spiking the membrane current can be caused by intrinsically electrical properties [Llinas, 2014] as well as synaptic input, whereas the fluctuation–driven spiking is exclusively caused by synaptic input. An intrinsic property, which is commonly believed to be involved in rhythm–generation, is the pacemaker property that can autonomously generate neuronal bursting in the absence of synaptic input [Brocard *et al.*, 2010]. The prominent presence of the fluctuation–regime therefore implies that the majority of neuronal spikes are not driven primarily by intrinsic properties such as pacemaker potentials, but rather by synaptic communication. This can be interpreted in two ways: 1) if there is a pacemaker–driven rhythmogenic core of oscillatory neurons responsible for the motor activity [Huckstepp *et al.*, 2016], the core only represents a small fraction of the network, or 2) since the fluctuation–regime is prominent and pacemaker neurons are difficult to find, the motor–rhythm may be generated by other means such as emergent collective processes in the network [Yuste, 2015]. Generation of movements without the need of pacemaker neurons have been predicted theoretically in central pattern generators [Kleinfeld and Sompolinsky, 1988] as well as more complex sequence generation [Hennequin *et al.*, 2014]. It remains to be understood how such distributed emergent processes can generate motor rhythms on a network level if, in fact, the pacemaker bursting is not an essential component.

Comparison with other parts of the CNS

Common features of network activity for different parts of the central nervous system may provide hints towards fundamental principles of neuronal operations. In the present study we identified the following features of population motor activity: 1) synaptic input to individual spinal neurons is normally distributed (**Figure 3F**, **supplement 2A**), 2) the means of these normal distributions are also normally distributed across the population. In particular, the distance to threshold in terms of fluctuations, i.e. $(V_m - V_{thres})/\sigma$ has a normal distribution and a distance from mean to threshold of 3σ on average (**Figure 3 supplement 3F**). 3) The neuronal response function is supralinear when the mean input is in the subthreshold region (**Figure 3H**, **supplement 2B**). 4) There is a rich diversity of regular to irregular spiking patterns. 5) The population firing rate is skewed and lognormal–like.

Many of these features have been identified before in other parts of CNS. The V_m of individual neurons is often normally distributed in cortical neurons when considering either the up– or down–state [Destexhe *et al.*, 2003; Stern *et al.*, 1997] and the spiking is irregular with a CV clustered around 1 [Softky and Koch, 1993; Stevens and Zador, 1998]. Similar irregularity is observed in non-vertebrates [Bruno *et al.*, 2015]. The distribution of mean CV_2 values in our experiments was clustered around 0.6 when ignoring the inter–burst intervals (**Figure 7C**). This is more regular than what is observed for typical cortical neurons, but similar to cervical interneurons in monkeys performing isometric wrist flexion–extensions [Prut and Perlmutter, 2003].

We observed a skewed and lognormal–like population distribution across behaviors (**Figure 6**, Movie supplement 1 and 2). Although, similar lognormal distributions have been reported in other parts of CNS [Buzsáki and Mizuseki, 2014; Hromádka *et al.*, 2008; O'Connor *et al.*, 2010; Wohrer *et al.*, 2013], it remains an open question how the skewness arises out of neuronal ensembles. *Roxin et al* [Roxin *et al.*, 2011] proposed a nonlinear transformation of Gaussian input as a mechanism (**Figure 1**). The minimal requirements for this to explain our observations are, first, a normally distributed input across neurons, second, a supralinear IO curve covering most of the input. Much of our data are in accordance with these requirements (**Figure 3F** and **supplement 3**) although some neurons do not have lognormal spiking. Notably, there is a distinction between the lognormal distribution mean rates across the population and the lognormal rate distribution of individual neurons. Whereas the lognormal population firing rate remains to be fully understood, the skewed firing rate distribution of individual neurons is fairly well understood. Here, the skewness is due to the fluctuating input and irregularity of spiking [Ostojic, 2011]. For instance, for lognormal–distributed ISIs, the skewness (ω) and CV are related as $\omega = (CV^2 + 3)CV$ [Ditlevsen and Lansky, 2011].

Fluctuation–driven regime as a subprimary range in motoneurons?

Classical studies of spinal motoneurons indicate two regimes of spiking: a primary and a secondary range [Kernell, 2006; Meehan *et al.*, 2010], which corresponds to different parts of the mean–driven spiking regime. This characterization was associated with the intrinsic properties without synaptic input being present. Nevertheless, a different type of fluctuation–driven spiking was discovered in experiments where synaptic input were present, in what was referred to the *subprimary range* in mice [Manuel and Heckman, 2011] and humans [Kudina, 1999; Matthews, 1996]. This subprimary range conforms to the fluctuation–regime though under a different terminology. As the name indicates, the primary range has been considered to represent the dominant mode of spiking whereas the subprimary range is a peculiarity. Nevertheless, a recent study recorded for the first time the motoneuron discharge and muscle force and found that the subprimary range accounts for 90% of the contraction force [Manuel and Heckman, 2011]. This indicates that the fluctuation–regime may have a more noteworthy role in covering the dynamical range in motor control than previously assumed.

Irregularity and sampling bias

In the present study, we use the metric CV_2 [Holt *et al.*, 1996] as a metric for local spiking irregularity, since it is widely used has been suggested as the most rate–invariant metric [Ponce-Alvarez *et al.*, 2010; Wohrer *et al.*, 2013]. We noticed a small difference in distribution of irregularity among the neurons recorded with intracellular versus extracellular electrodes (data not shown). The neurons were recorded with intracellular electrodes had more regular spiking than those recorded with extracellular electrodes. This may be caused by a systematic bias in the way the intracellularly recorded neurons were collected, as there is an experimental bias towards high firing rates. Spike sorting processing of the extracellular recordings, on the other hand, is likely to both miss spikes and contain false positives, which will cause overestimation of spiking irregularity.

Materials and Methods

Experimental procedures

We used the integrated turtle preparation with the spinal motor network intact ($n = 5$ for the multi–electrode recordings and $n = 60$ for the serially aqquired intracellular recordings), in order to address how the neuronal firing rates are distributed across the population of interneurons and motoneurons in the spinal cord [Petersen *et al.*, 2014]. These sample sizes where assumed to be large enough in the experimental design and because

of a consistency in results, although a specific power analysis was not conducted. To avoid the confounding factors of supraspinal input, we spinalized the turtle. The transection was performed at the spinal cord at segments (D3-4) caudal to the cervical segments, where the local circuitry has only little or no involvement in generation of motor patterns [Hao *et al.*, 2014; Mortin and Stein, 1989; Mui *et al.*, 2012]. The adult turtle preparation is capable of producing elaborate motor patterns such as scratching. We used the semi-intact spinal cord of adult turtles [Keifer and Stein, 1983; Petersen *et al.*, 2014] and recorded from the segments D8-D10. These segments contain the essential CPG circuits [Mortin and Stein, 1989]. Most of the spinal cord including the sensory periphery is left intact. The blood is replaced and the spinal column is provided with oxygenated Ringers solution so that the neurons and the network have optimal conditions. In this experimental situation the motor behavior is as close to *in vivo* situation as possible, and is indistinguishable from the intact condition [Keifer and Stein, 1983]. The turtle preparation allow for mechanical stability and the turtle's resistance to anoxia allow for remarkable durability of both the recording conditions and the motor pattern reproducibility [Vestergaard and Berg, 2015].

Integrated Preparation Adult red-eared turtles (*Trachemys scripta elegans*) of either sex were placed on crushed ice for 2 hours to ensure hypothermic anesthesia. The turtles were killed by decapitation and the blood was substituted by the perfusion with a Ringer's solution containing (mM): 100 NaCl; 5 KCl; 30 $NaHCO_3$; $2MgCl_2$; $3CaCl_2$; and 10 glucose, saturated with 95% O_2 and 5% CO_2 to obtain pH 7.6, to remove the blood from the nervous system. We isolated the carapace containing the spinal cord segments D4-Ca2 by transverse cuts [Keifer and Stein, 1983; Petersen *et al.*, 2014] and perfused the cord with Ringer's solution through the *vertebral foramen*, using a steel tube and gasket pressing against the D4 vertebra. We opened the spinal column on the ventral side along D8-D10 and gently removed the dura mater with a fine scalpel and forceps. For each insertion site for the silicon probed, we opened the pia mater with longitudinal cuts along the spinal cord with the tip of a bend syringe needle tip (BD Microlance 3: $27G3/4$",$0.4x19mm$). We performed the cuts parallel to the ventral horn between the ventral roots. The surgical procedures comply with Danish legislation and were approved by the controlling body under the Ministry of Justice.

Network Activation We used a fire polished tip of a bent glass rod for mechanical stimulation, that was mounted linear actuator. The actuator was controlled with a function generator: frequency, amplitude and duration of the stimulus.

Extracellular Recordings Extracellular recordings were performed in parallel at $40kHz$ using a 256 channel multiplexed Amplipex amplifier (KJE-1001, Amplipex). Up to four 64-channel silicon probes were inserted in the incisions perpendicular to the spinal cord from the ventral side. We used the 64-channel Berg silicon probes (Berg64 from NeuroNexus Inc., Ann Arbor, MI, USA) with 8 shanks, and 8 recording sites on each shank arranged in a staggered configuration with $30\mu m$ vertical distance. The shanks are distanced $200\mu m$ apart. Recordings were performed at depths in the range of 400-1000μm.

Intracellular Recordings The intracellular recordings were performed in current-clamp mode with an Axon Multiclamp 700B amplifier (Molecular devices). Glass pipettes were pulled with a P-1000 puller (Sutter instruments) and filled with a mixture of 0.9 M potassium acetate and 0.1 M KCl. Data were sampled at about 20 kHz with a 12-bit analog-to-digital converter (Axon Digidata 1440a, Molecular devices). We inserted the glass electrodes from the ventral side of D8-D10 perpendicularly to the spinal cord. Neurons were located at depths ranging from about 300-800μm. Typically we had stable intracellular recordings for multiple trials.

Nerve Recordings Electroneurogram (ENG) recordings were performed with suction electrodes. The scratch behavior was measured by the activity of the nerves: Hip Flexor, Knee Extensor, dD8 and HR-KF. The nerve activities were recorded with a differential amplifier Iso-DAM8 (World Precision Instruments) with bandwidth of $100Hz - 1kHz$.

Histology For histological verification, we combined several staining techniques: The silicon probes were painted with DiI ($1-2\%$ diluted in ethanol) before insertion into the spinal cord [Blanche *et al.*, 2005;

Vandecasteele *et al.*, 2011]. Following successful experiments, we performed Nissl– and ChAT–staining of the tissue, to determine the location of respectively neurons and motoneurons.

The histological processing is detailed in Petersen *et al.* [2014]. We carefully removed the tissue, perfused it and put it in phosphate buffered saline (PBS) with 4% paraformaldehyde for 24–48 hrs and further stored it in PBS. The tissue was mounted in an agar solution and sliced into $100\mu m$ slices using a microtome (Leica, VT1000 S). The slices were washed with PBS and incubated overnight at 5^oC with primary choline acetyltransferase antibodies goat anti-ChAT antibodies (1:500, Milipore, USA) in blocking buffer, which is PBS with 5% donkey serum and 0.3% Triton X-100. The slices were washed three times with PBS and incubated for 1 hr at room temperature with the secondary antibody Alexa488 conjugated to donkey anti-goat antibodies (1:1000 Jackson) in blocking buffer. After three washes with PBS, the slice was mounted on cover slit with a drop of ProLong Gold antifade reagent (Invitrogen Molecular Probes, USA) and cured overnight at room temperature before microscopy. The slice was viewed using a confocal microscope, Zeiss LSM 700 with diode lasers, on a Zeiss Axiolmager M2 using 10x/0.30 EC Plan-Neofluar, 40x/0.6 Corr LD Plan-Neofluar, and 63x/1.40 oil DIC Plan-Apochromat objectives (Zeiss).

Data Analysis

The data analysis was primarily done in the programming languages Matlab and Python. The correlation coefficient was calculated as the Pearson product-moment correlation coefficient.

Skewness of distribution We use *skewness* [Press *et al.*, 1992] or the third moment as a measure of asymmetry in the distribution around the mean, sometimes referred to as Pearson's moment coefficient of skewness. It can be estimated using the method of moment estimator as

$$Skewness = \frac{1}{N}\sum_{j=1}^{N}\left[\frac{x_j - \bar{x}}{\sigma}\right]^3 \tag{1}$$

where $x_1, ..., x_N$ are all the observations (V_m or firing rate) and σ and $\bar{x}$ are the sample standard deviation and sample mean of the distribution. The skewness is a unitless number and a value of zero indicates perfect symmetry. A positive skew has a tale pointing in the positive direction of the axis and a negative value points in the opposite direction.

Spike Sorting Spike sorting was performed in the Klustakwik-suite: SpikeDetekt, KlusterKwik v.3.0 and KlustaViewa [Kadir *et al.*, 2014]. Raw extracellular signals were bandpass filtered from $400 - 9000Hz$, and spikes were detected by a median based amplitude threshold with SpikeDetekt [Kadir *et al.*, 2014; Quiroga *et al.*, 2004; Takekawa *et al.*, 2012]. An automatic clustering of the spikes was performed in KlustaKwik, followed by manual cluster-cutting and cluster verification in KlustaViewa. The cluster quality was evaluated by several measures: The shape of the autocorrelation function, the amount of contamination in the refractory period, the Isolation distance [Harris *et al.*, 2001] and the L_{ratio} [Schmitzer-Torbert and Redish, 2004] (**Figure 2 supplement 2**). Only well isolated units was used in the further data analysis.

Time-dependent Firing Rates The time-dependent firing rate were estimated by a gaussian kernel. Spike times $x(t)$ were convoluted with a kernel $k(t)$ to estimate the instantaneous firing rate

$$rate(t) = \int_{-\infty}^{\infty} x(t - t')k(t')dt' \tag{2}$$

where $k(t)$ is defined as

$$k(t) = \frac{1}{\sqrt{2\pi}\omega}e^{-\frac{t^2}{2\omega^2}} \tag{3}$$

with the bandwidth ω optimized for each spiketrain with the sskernel method [Shimazaki and Shinomoto, 2010]. The estimated width was in the range of $100 - 500\mu s$.

Gini Coefficient The *Gini* coefficient is a measure of statistical dispersion and it is defined as a ratio of the areas on the Lorenz curve diagram

$$Gini = \frac{a}{a+b} = 1 - 2b \tag{4}$$

where $a + b$ is the area below the line of no dispersion (the diagonal, i.e. $a + b = 1/2$), and b is the Lorenz curve, i.e. the cumulative distribution of firing rates (**Figure 6H**).

Irregularity of the Spiking Activity The irregularity of the spiking of individual neurons can be described by several measures. The most common measures are the coefficient of variation ($CV = \sigma/\mu$) and the Fano factor ($F = \sigma^2/\mu$), but both measures easily overestimate the irregularity when the firing rate is non-stationary [Holt *et al.*, 1996; Ponce-Alvarez *et al.*, 2010; Softky and Koch, 1993]. More advanced methods of estimating the time dependent variations in the irregularity have been developed [Miura *et al.*, 2006; Shimokawa and Shinomoto, 2009; Shinomoto *et al.*, 2009], but here we use the widely used metric CV_2, which has been suggested to be the most robust measure of local spiking irregularity [Ponce-Alvarez *et al.*, 2010; Wohrer *et al.*, 2013]. The time dependent CV_2 is defined by pairs of adjacent inter-spike intervals ISI_i and ISI_{i+1}:

$$CV_2(i) = \frac{2|ISI_i - ISI_{i+1}|}{ISI_i + ISI_{i+1}} \tag{5}$$

where $CV_2 = 1$ for a Poisson process and $CV_2 = 0$ for a regular process. CV_2 can take values in the range from zero to two.

TIF_{50} and SIF_{50}: time and spikes in fluctuation regime based on spiking irregularity To get a quantitative handle on the fraction of neurons found in the fluctuation–regime across the population, we consider the distribution of neurons, $f(t)$, which spends a given amount of normalized time t in the fluctuation regime, i.e. with $CV_2 > i_{crit}$. We consider three values of i_{crit}, 0.4, 0.5 and 0.6, as indicators for when the neurons are in the fluctuation–regime. Formally we quantify the time in fluctuation–regime for the population using the reverse cumulative distribution of neurons (**Figure 7D–E** and **supplement 1**). The reverse cumulative fraction of neurons in the fluctuation regime $F(t)$ for a given fraction of normalized time t is

$$F(t) = 1 - \int_0^t f(t)dt,\ 0 < t \leq 1 \tag{6}$$

This fraction $F(t)$ is the fraction of neurons, which spend at least t amount of normalized time in the fluctuation regime. To compress the distribution into a single number we use the fraction of time in fluctuation regime of half of the population, TIF_{50}, which is the value of t for which $F(t) = 50\%$ (arrows and broken lines, **Figure 7D–E**).

Since the firing rate is rarely constant, one may want to know how many spikes are elicited in the mean– versus fluctuation regime. This is calculated in similar way, using the distribution of neurons having a normalized fraction of spikes in the fluctuation regime, i.e. spikes with $CV_2 > i_{crit}$, $f(s)$. The reverse cumulative of $f(s)$ again gives the fraction of neurons which have at least s spikes in fluctuation regime, normalized to 100%,

$$F(s) = 1 - \int_0^s f(s)dt,\ 0 < s \leq 1 \tag{7}$$

Again we compress the distribution into a single number and use the fraction of spikes, which occur in fluctuation regime of half of the population, SIF_{50}, which is the value of s for which $F(s) = 50\%$ (arrows and broken lines **Figure 7 supplement 1**).

Estimating threshold Based on the method by Sekerli *et al.* [2004]. In this paper they suggest two methods of estimating threshold. Here we use the first method, which is based on revealing the threshold in a phase plot of V_m versus the derivative dV_m/dt. The largest positive slope of V_m versus the derivative dV_m/dt in the trace leading up to the spike peak is an indication of the threshold. The V_m trace is low pass filtering at 5000 Hz.

Spike rate versus V_m (FV-curve) The method for estimating the response rate as a function of V_m has been described previously [Vestergaard and Berg, 2015]. First, we empirically determine the stochastic distribution of V_m prior to the spike (1.5-1.7 ms prior) of neurons in the fluctuation–driven regime (as assessed by the return map method). Then we normalize this distribution with the total amount of time spent at each V_m-level at all time. This is the probability of getting a spike within a small time window for a given membrane potential. This is empirical probability of getting a spike in a short time–window, i.e. the spike rate, as a function of V_m [Jahn *et al.*, 2011]. It is analogous to poisson processes under the assumption that the spiking can be considered a renewal process. The shape of the spike response function is highly non-linear with upward curvature. This has been observed in previous experiments often referred to as expansive non-linearity [Hansel and van Vreeswijk, 2002; Miller and Troyer, 2002; Murphy and Miller, 2003; Priebe and Ferster, 2005, 2008]. An exponential

$$R(V_m) = ce^{\beta V_m} \tag{8}$$

was fitted to capture the curvature, where the curvature is represented in the exponent β, which have units of $1/mV$, and c is a constant of units $1/s$. Such expansive non-linearities have also been investigated in the visual cortex where they are often characterized as a power-law relationship, i.e.

$$R(V_m) = k[V_m - E_a]^{\alpha} \tag{9}$$

where α is the scaling parameter > 1, i.e. supralinear, and often ranging from 2-5 [Hansel and van Vreeswijk, 2002; Miller and Troyer, 2002]. This exponent is also a measure of the expansive curvature of the non-linearity. E_a represent a subthreshold level of V_m, where the spiking probability is zero, such that the values in the sampled traces are always larger than E_a, i.e. $V_m > E_a$. The curvature dependence on synaptic fluctuations was assessed by the standard deviation of the distribution of V_m traces prior to the spike in the diffusion regime, i.e. where there was no link to the V_m and the spike occurrence. This distribution was chosen 15 ms prior to the spike (Figure 2). The analysis and fits were performed in Matlab with generic fitting functions.

Return Map Ratio: Intracellular metric for mean– vs. fluctuation–regime In order to distinguish neurons in fluctuation– versus mean–regime, we employ a new metric for quantifying the degree of fluctuations in V_m in between action potentials. We plot the values of V_m in a return map, which is a plot of $V_m(t)$ versus $V_m(t + \Delta t)$. If the inter–spike V_m has a direct trajectory from the reset potential to the next spike, V_m will smoothly increase and thus $V_m(t + \Delta t)$ will always be larger $V_m(t)$. Therefore each point will be above the line of unity (**Figure 3 supplement 1A–B**). On the other hand, if V_m has fluctuations, it will have an indirect and convolved trajectory from the reset value to the threshold. This will manifest as containing values of $V_m(t+\Delta t)$ which are actually smaller than $V_m(t)$. Thus we use the ratio of points above versus below the unity line as a metric for how convolved and fluctuating the path of V_m is from reset to threshold. If the ratio is $\sim$0.5 V_m is highly fluctuating, whereas if the ratio is approaching 1 the path is straight without any fluctuations. We choose a mean value of the histogram of all values to 0.7 to classify neurons as fluctuation– or mean–driven (**Figure 3 supplement 1C**). This metric of straight versus convolved trajectory had significant negative correlation with other measures of fluctuation– regime, e.g. spike rate skewness, spike irregularity (CV_2) and *least time below threhold* (LTBT, **Figure 3 supplement 1D–F**). The choice of Δt is not important as long as it is larger than the timescale of electronic fluctuations of the amplifiers and smaller than the timescale of synaptic fluctuations in V_m. We consistently used $\Delta t = 1.5$ ms for all neurons.

Data selection

In figure 6 was used the following trials: $n = [6, 4, 9, 5, 6]$ for ipsilateral pocket scratch and $n = [6, 3, 10, 5, 6]$ for contralateral pocket scratch. Data used in **Figure 5A–F** has already been published in a different context [Berg *et al.*, 2007]. A small subset of the neurons used in **Figure 3B** ($n = 10$ out of 68) has been acquired in a reduced preparation [Petersen *et al.*, 2014] and published for an investigation of a different matter [Berg *et al.*, 2007, 2008]. The data from experiments of blockade of inhibition using superfusion of strychnine has also been published previously in the investigation of a different matter [Vestergaard and Berg, 2015].

AUTHOR CONTRIBUTIONS

Conceptualization, Methodology, Investigation, Software, Visualization, P.C.P. and R.W.B.; Formal Analysis P.C.P.; Writing–Original Draft, Funding Acquisition, Supervision, R.W.B.

ACKNOWLEDGEMENTS

Thanks to György Buzsáki, Daniel F. English and Henrik Lindén for reading and commenting on an earlier version of the manuscript. Funded by Novo Nordisk Foundation (RB), the Danish Council for Independent Research Medical Sciences (RB and PP) and the Dynamical Systems Interdisciplinary Network, University of Copenhagen.

References

Ahmadian, Y., Rubin, D. B., and Miller, K. D. (2013). Analysis of the stabilized supralinear network. *Neural Comput*, **25**, 1994–2037.

Amit, D. J. and Brunel, N. (1997). Model of global spontaneous activity and local structured activity during delay periods in the cerebral cortex. *Cerebral cortex*, **7**(3), 237–52.

Anderson, J. S., Lampl, I., Gillespie, D. C., and Ferster, D. (2000). The contribution of noise to contrast invariance of orientation tuning in cat visual cortex. *Science*, **290**(5498), 1968–1972.

Berg, R. W., Alaburda, A., and Hounsgaard, J. (2007). Balanced inhibition and excitation drive spike activity in spinal half-centers. *Science*, **315**(5810), 390–3.

Berg, R. W., Ditlevsen, S., and Hounsgaard, J. (2008). Intense synaptic activity enhances temporal resolution in spinal motoneurons. *PLoS one*, **3**(9), e3218.

Berkowitz, A., Roberts, A., and Soffe, S. R. (2010). Roles for multifunctional and specialized spinal interneurons during motor pattern generation in tadpoles, zebrafish larvae, and turtles. *Front Behav. Neurosci.*, **4**(June), 36.

Blanche, T. J., Spacek, M. A., Hetke, J. F., and Swindale, N. V. (2005). Polytrodes: high-density silicon electrode arrays for large-scale multiunit recording. *J. Neurophysiol.*, **93**(5), 2987–3000.

Britz, O., Zhang, J., Grossmann, K. S., Dyck, J., Kim, J. C., Dymecki, S., Gosgnach, S., and Goulding, M. (2015). A genetically defined asymmetry underlies the inhibitory control of flexor-extensor locomotor movements. *eLife*, **4**(e04718), 1–22.

Brocard, F., Tazerart, S., and Vinay, L. (2010). Do pacemakers drive the central pattern generator for locomotion in mammals? *The Neuroscientist : a review journal bringing neurobiology, neurology and psychiatry*, **16**(2), 139–55.

Brunel, N. (2000). Dynamics of networks of randomly connected excitatory and inhibitory spiking neurons. *J Physiol Paris*, **94**(5-6), 445–63.

Bruno, A. M., Frost, W. N., and Humphries, M. D. (2015). Modular deconstruction reveals the dynamical and physical building blocks of a locomotion motor program. *Neuron*, **86**(1), 304–318.

Buzsáki, G. and Mizuseki, K. (2014). The log-dynamic brain: how skewed distributions affect network operations. *Nat Rev Neurosci*, (February), 1–15.

Destexhe, A., Rudolph, M., and Paré, D. (2003). The high-conductance state of neocortical neurons in vivo. *Nat Rev Neurosci*, **4**(9), 739–51.

Ditlevsen, S. and Lansky, P. (2011). Firing variability is higher than deduced from the empirical coefficient of variation. *Neural Comput*, **23**(8), 1944–66.

Gerstner, W., Kistler, W. M., Naud, R., and Paninski, L. (2014). *Neuronal Dynamics: From Single Neurons to Networks and Models of Cognition*. Cambridge University Press, New York, NY, USA.

Hansel, D. and Mato, G. (2001). Existence and Stability of Persistent States in Large Neuronal Networks. *Phys Rev Lett*, **86**(18), 4175–4178.

Hansel, D. and van Vreeswijk, C. (2002). How noise contributes to contrast invariance of orientation tuning in cat visual cortex. *J Neurosci*, **22**(12), 5118–28.

Hao, Z., Meier, M., and Berkowitz, A. (2014). Rostral spinal cord segments are sufficient to generate a rhythm for both locomotion and scratching but affect their hip extensor phases differently. *J Neurophysiol*, **112**(1), 147–155.

Harris, K. D., Hirase, H., Leinekugel, X., Henze, D. A., and Buzsáki, G. (2001). Temporal interaction between single spikes and complex spike bursts in hippocampal pyramidal cells. *Neuron*, **32**(1), 141–149.

Hennequin, G., Vogels, T. P., and Gerstner, W. (2014). Optimal control of transient dynamics in balanced networks supports generation of complex movements. *Neuron*, **82**(6), 1394–1406.

Holt, G. R., Softky, W. R., Koch, C., and Douglas, R. J. (1996). Comparison of discharge variability in vitro and in vivo in cat visual cortex neurons. *J Neurophysiol*, **75**(5), 1806–1814.

Hromádka, T., DeWeese, M. R., and Zador, A. M. (2008). Sparse representation of sounds in the unanesthetized auditory cortex. *PLoS Biology*, **6**(1), 0124–0137.

Huckstepp, R. T., Henderson, L. E., Cardoza, K. P., and Feldman, J. L. (2016). Interactions between respiratory oscillators in adult rats. *eLife*, **5**(e14203), 1–22.

Ikegaya, Y., Sasaki, T., Ishikawa, D., Honma, N., Tao, K., Takahashi, N., Minamisawa, G., Ujita, S., and Matsuki, N. (2013). Interpyramid spike transmission stabilizes the sparseness of recurrent network activity. *Cereb Cortex*, **23**(2), 293–304.

Jahn, P., Berg, R. W., Hounsgaard, J., and Ditlevsen, S. (2011). Motoneuron membrane potentials follow a time inhomogeneous jump diffusion process. *J. comput. neurosci.*, **31**(3), 563–79.

Kadir, S. N., Goodman, D. F. M., and Harris, K. D. (2014). High-dimensional cluster analysis with the masked EM algorithm. *Neural computation*, **26**(11), 2379–94.

Keifer, J. and Stein, P. S. (1983). In vitro motor program for the rostral scratch reflex generated by the turtle spinal cord. *Brain research*, **266**(1), 148–51.

Kernell, D. (2006). *The motoneurone and its muscle fibres*. Oxford University Press, New York.

Kleinfeld, D. and Sompolinsky, H. (1988). Associative neural network model for the generation of temporal patterns. Theory and application to central pattern generators. *Biophys J*, **54**, 1039–1051.

Kolind, J., Hounsgaard, J., and Berg, R. W. (2012). Opposing effects of intrinsic conductance and correlated synaptic input on Vm-fluctuations during network activity. *Front. Comput. Neurosci.*, **6**(40).

Koulakov, A. A., Hromádka, T., and Zador, A. M. (2009). Correlated connectivity and the distribution of firing rates in the neocortex. *J Neurosci*, **29**(12), 3685–94.

Kudina, L. P. (1999). Analysis of firing behaviour of human motoneurones within 'subprimary range'. In *J Physiol Paris*, volume 93, pages 115–123.

Kuhn, A., Aertsen, A., and Rotter, S. (2004). Neuronal integration of synaptic input in the fluctuation-driven regime. *J. Neurosci.*, **24**(10), 2345–56.

Kumar, A., Schrader, S., Aertsen, A., and Rotter, S. (2008). The high-conductance state of cortical networks. *Neural Comput*, **20**(1), 1–43.

Llinas, R. R. (2014). Intrinsic electrical properties of mammalian neurons and CNS function: a historical perspective. *Front. Cell. Neurosci.*, **8**, 320.

Manuel, M. and Heckman, C. J. (2011). Adult Mouse Motor Units Develop Almost All of Their Force in the Subprimary Range: A New All-or-None Strategy for Force Recruitment? *J Neurosci*, **31**(42), 15188–15194.

Matthews, P. B. (1996). Relationship of firing intervals of human motor units to the trajectory of post-spike after-hyperpolarization and synaptic noise. *J Physiol*, **492 (Pt 2**(1996), 597–628.

Meehan, C. F., Sukiasyan, N., Zhang, M., Nielsen, J. B., and Hultborn, H. (2010). Intrinsic properties of mouse lumbar motoneurons revealed by intracellular recording in vivo. *J Neurophysiol*, **103**(5), 2599–2610.

Miller, K. D. and Troyer, T. W. (2002). Neural noise can explain expansive, power-law nonlinearities in neural response functions. *J neurophysiol*, **87**(2), 653–9.

Miura, K., Okada, M., and Amari, S.-I. (2006). Estimating spiking irregularities under changing environments. *Neural Comput*, **18**(10), 2359–86.

Mizuseki, K. and Buzsáki, G. (2013). Preconfigured, skewed distribution of firing rates in the hippocampus and entorhinal cortex. *Cell Reports*, **4**(5), 1010–1021.

Mortin, L. I. and Stein, P. S. (1989). Spinal cord segments containing key elements of the central pattern generators for three forms of scratch reflex in the turtle. *J. Neurosci.*, **9**(7), 2285–96.

Mui, J. W., Willis, K. L., Hao, Z. Z., and Berkowitz, A. (2012). Distributions of active spinal cord neurons during swimming and scratching motor patterns. *Journal of Comparative Physiology A: Neuroethology, Sensory, Neural, and Behavioral Physiology*, **198**(12), 877–889.

Murphy, B. K. and Miller, K. D. (2003). Multiplicative gain changes are induced by excitation or inhibition alone. *J. Neurosci.*, **23**(31), 10040–51.

O'Connor, D. H., Peron, S. P., Huber, D., and Svoboda, K. (2010). Neural activity in barrel cortex underlying vibrissa-based object localization in mice. *Neuron*, **67**(6), 1048–1061.

Okun, M. and Lampl, I. (2009). Balance of excitation and inhibition. *Scholarpedia*, **4**(8), 7467.

Ostojic, S. (2011). Interspike interval distributions of spiking neurons driven by fluctuating inputs. *J Neurophysiol*, **106**(1), 361–373.

Ozeki, H., Finn, I. M., Schaffer, E. S., Miller, K. D., and Ferster, D. (2009). Inhibitory stabilization of the cortical network underlies visual surround suppression. *Neuron*, **62**(4), 578–92.

Petersen, P. C., Vestergaard, M., Jensen, K. H. R., and Berg, R. W. (2014). Premotor Spinal Network with Balanced Excitation and Inhibition during Motor Patterns Has High Resilience to Structural Division. *J Neurosci*, **34**(8), 2774–2784.

Ponce-Alvarez, A., Kilavik, B. E., and Riehle, A. (2010). Comparison of local measures of spike time irregularity and relating variability to firing rate in motor cortical neurons. *J Comput Neurosci*, **29**(1-2), 351–365.

Powers, R. K. and Binder, M. D. (2000). Relationship between the time course of the afterhyperpolarization and discharge variability in cat spinal motoneurones. *J Physiol*, **528 Pt 1**(2000), 131–50.

Press, W., Teukolsky, S., Vetterling, W., and Flannery, B. (1992). *Numerical Recipes in FORTRAN: The Art of Scientific Computing*. Cambridge University Press.

Priebe, N. J. and Ferster, D. (2005). Direction selectivity of excitation and inhibition in simple cells of the cat primary visual cortex. *Neuron*, **45**(1), 133–45.

Priebe, N. J. and Ferster, D. (2008). Inhibition, spike threshold, and stimulus selectivity in primary visual cortex. *Neuron*, **57**(4), 482–97.

Prut, Y. and Perlmutter, S. I. (2003). Firing properties of spinal interneurons during voluntary movement. I. State-dependent regularity of firing. *J Neurosci*, **23**(29), 9600–10.

Quiroga, R. Q., Nadasdy, Z., and Ben-Shaul, Y. (2004). Unsupervised spike detection and sorting with wavelets and superparamagnetic clustering. *Neural computation*, **16**(8), 1661–1687.

Renart, A., Moreno-Bote, R., Wang, X.-J., and Parga, N. (2007). Mean-driven and fluctuation-driven persistent activity in recurrent networks. *Neural Comput*, **19**(1), 1–46.

Richardson, M. J. E. and Gerstner, W. (2006). Statistics of subthreshold neuronal voltage fluctuations due to conductance-based synaptic shot noise. *Chaos*, **16**(2), 026106.

Roxin, A., Brunel, N., Hansel, D., Mongillo, G., and van Vreeswijk, C. (2011). On the distribution of firing rates in networks of cortical neurons. *J Neurosci*, **31**(45), 16217–26.

Rubin, D. B., Hooser, S. D. V., and Miller, K. D. (2015). The stabilized supralinear network : A unifying circuit motif underlying multi-input integration in sensory cortex. *Neuron*, **85**, 402–417.

Schmitzer-Torbert, N. and Redish, A. D. (2004). Neuronal activity in the rodent dorsal striatum in sequential navigation: separation of spatial and reward responses on the multiple T task. *Journal of neurophysiology*, **91**(5), 2259–2272.

Sekerli, M., Del Negro, C. A., Lee, R. H., and Butera, R. J. (2004). Estimating action potential thresholds from neuronal time-series: New metrics and evaluation of methodologies. *IEEE Transactions on Biomedical Engineering*, **51**(9), 1665–1672.

Shadlen, M. N. and Newsome, W. T. (1994). Noise, neural codes and cortical organization. *Curr Opin Neurobiol*, **4**(4), 569–79.

Shadlen, M. N. and Newsome, W. T. (1998). The variable discharge of cortical neurons: implications for connectivity, computation, and information coding. *J. Neurosci.*, **18**(10), 3870–96.

Shimazaki, H. and Shinomoto, S. (2010). Kernel bandwidth optimization in spike rate estimation. *J. comput. neurosci.*, **29**(1-2), 171–82.

Shimokawa, T. and Shinomoto, S. (2009). Estimating instantaneous irregularity of neuronal firing. *Neural Comput*, **21**(7), 1931–1951.

Shinomoto, S., Kim, H., Shimokawa, T., Matsuno, N., Funahashi, S., Shima, K., Fujita, I., Tamura, H., Doi, T., Kawano, K., Inaba, N., Fukushima, K., Kurkin, S., Kurata, K., Taira, M., Tsutsui, K.-I., Komatsu, H., Ogawa, T., Koida, K., Tanji, J., and Toyama, K. (2009). Relating Neuronal Firing Patterns to Functional Differentiation of Cerebral Cortex. *PLoS Comput Biol*, **5**(7), e1000433.

Silver, R. A. (2010). Neuronal arithmetic. *Nat Rev Neurosci*, **11**(7), 474–89.

Softky, W. R. and Koch, C. (1993). The highly irregular firing of cortical cells is inconsistent with temporal integration of random EPSPs. *J. Neurosci.*, **13**(1), 334–50.

Song, S., Sjostrom, P. J., Reigl, M., Nelson, S., and Chklovskii, D. B. (2005). Highly nonrandom features of synaptic connectivity in local cortical circuits. In *PLoS Biology*, volume 3, pages 0507–0519.

Stein, P. (2005). Neuronal control of turtle hindlimb motor rhythms. *J Comp Physiol A Neuroethol Sens Neural Behav Physiol*, **191**, 213–229.

Stern, E. a., Kincaid, a. E., and Wilson, C. J. (1997). Spontaneous subthreshold membrane potential fluctuations and action potential variability of rat corticostriatal and striatal neurons in vivo. *J. Neurophysiol.*, **77**(4), 1697–715.

Stevens, C. F. and Zador, a. M. (1998). Input synchrony and the irregular firing of cortical neurons. *Nat Neurosci*, **1**(3), 210–7.

Takekawa, T., Isomura, Y., and Fukai, T. (2012). Spike sorting of heterogeneous neuron types by multimodality-weighted PCA and explicit robust variational Bayes.

Tiesinga, P. H. E., José, J. V., and Sejnowski, T. J. (2000). Comparison of current-driven and conductance-driven neocortical model neurons with Hodgkin-Huxley voltage-gated channels. *Phys Rev E*, **62**(6), 8413–8419.

van Vreeswijk, C. and Sompolinsky, H. (1998). Chaotic balanced state in a model of cortical circuits. *Neural Comput*, **10**(6), 1321–1371.

Vandecasteele, M., Deniau, J. M., and Venance, L. (2011). Spike frequency adaptation is developmentally regulated in substantia nigra pars compacta dopaminergic neurons. *Neuroscience*, **192**, 1–10.

Vestergaard, M. and Berg, R. W. (2015). Divisive Gain Modulation of Motoneurons by Inhibition Optimizes Muscular Control. *J Neurosci*, **35**(8), 3711–3723.

Vogels, T. P., Rajan, K., and Abbott, L. F. (2005). Neural network dynamics. *Annu Rev Neurosci*, **28**(March), 357–76.

Wohrer, A., Humphries, M. D., and Machens, C. K. (2013). Population-wide distributions of neural activity during perceptual decision-making. *Prog Neurobiol*, **103**, 156–193.

Young, E. D., Robert, J. M., and Shofner, W. P. (1988). Regularity and latency of units in ventral cochlear nucleus: implications for unit classification and generation of response properties. *J Neurophysiol*, **60**(1), 1–29.

Yuste, R. (2015). From the neuron doctrine to neural networks. *Nat Rev Neurosci*, **16**(8), 487–497.

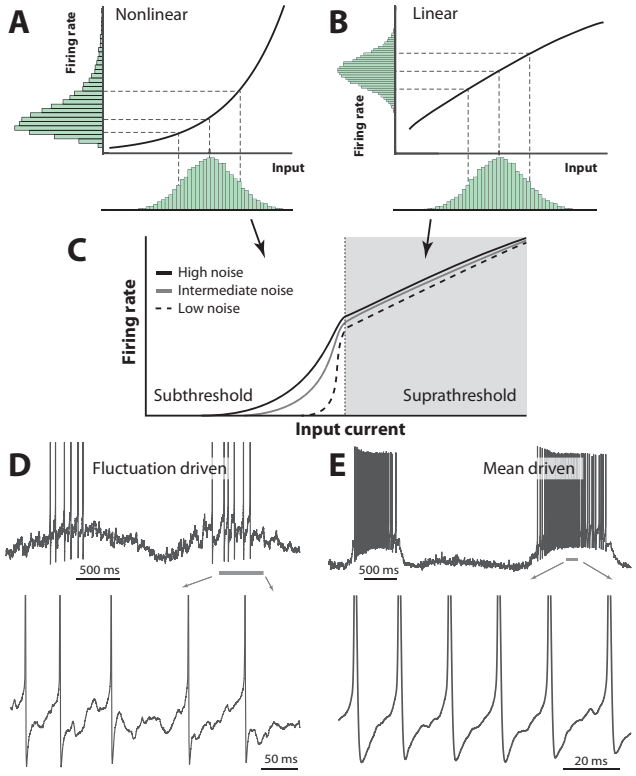

Figure 1: Skewness of the rate distribution reveals two regimes of neuronal spiking. (A) In the fluctuation–driven regime the mean input is below the spiking threshold and the IO-curve has a nonlinear shape. A normally distributed input current (shown below x–axis) is transformed into a skewed firing rate distribution (y-axis). (B) In contrast, if the mean input is above threshold, the transformation is linear and the firing rate distribution is symmetric. (C) IO–function for both regimes. The noise level affects the curvature of the nonlinearity. Adapted from [Roxin *et al.*, 2011]. (D) Sample recordings during motor activity from two spinal neurons in the subthreshold region, where the spiking is irregular and driven by fluctuations, and the supra–threshold region (E), where the mean input is above threshold and spiking is regular. Highlighted area shown at bottom. Spikes in bottom panel are clipped.

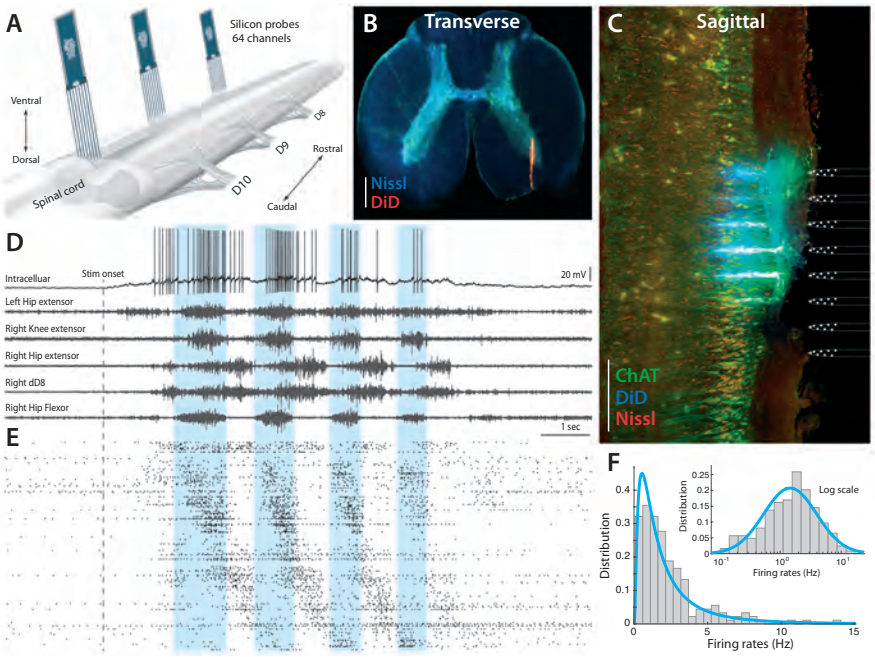

Figure 2: Parallel neuronal activity in the lumbar enlargement during rhythmic motor activity. (**A**) Illustration of experiment with three silicon probes inserted into the lumbar spinal cord of a turtle. Histological verification: transverse (**B**) and sagittal (**C**) slices, 200μm thick, showing the location of the silicon probes in the spinal cord (red traces and location illustrated on right, electrodes stained with DiD). ChAT staining in green and Nissl stain in blue. (**D**) V_m of a single neuron (top) concurrently recorded with five motor nerves (traces below) during scratching behavior induced by a somatic touch (onset indicated, 10-s duration). (**E**) Rastergram showing the parallel-recorded single units (∼200 neurons) sorted according to hip flexor phase. (**F**) Firing rate distribution is positively skewed and lognormal–like (inset). For details, see Figure supplement 1 and 2.

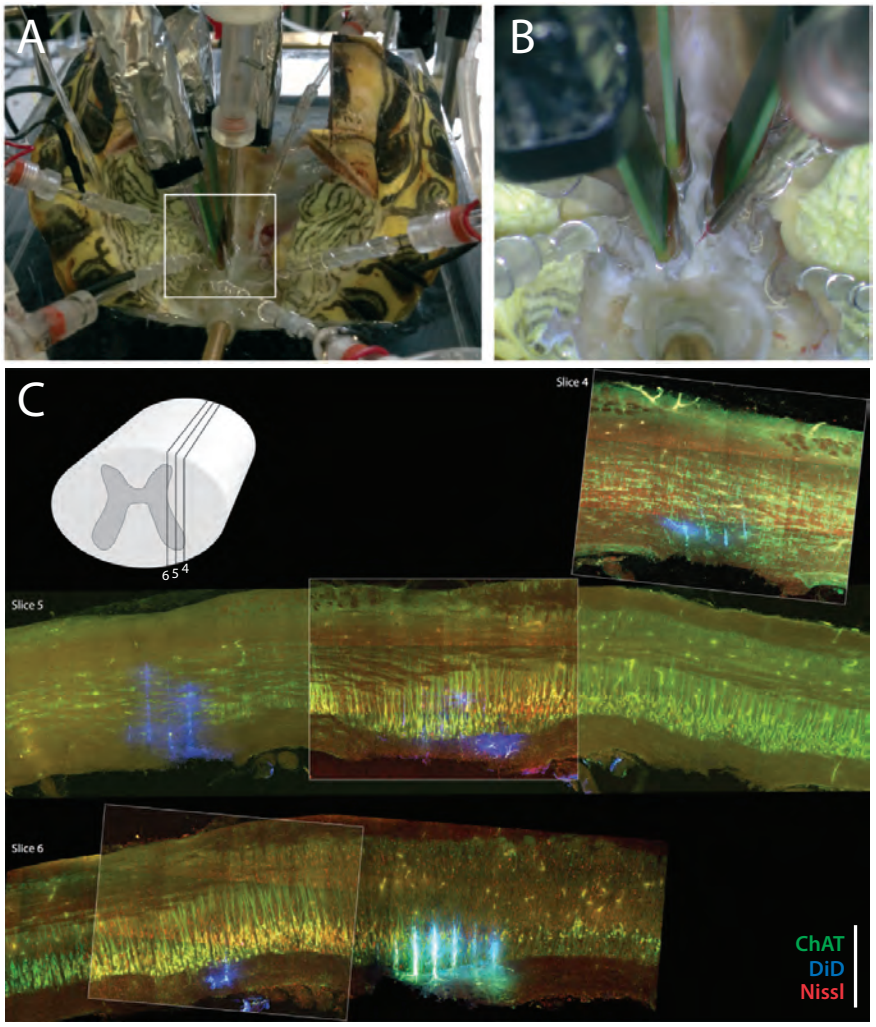

figure supplement 1: Experimental setup. (**A**) Picture of the preparation with electrodes inserted into the spinal cord of a turtle, which is lying on its back with the caudal part of the carapace and spinal cord intact. The scratch reflex motor pattern is activated by the mechanical touch of the carapace with a glass rod attached to an actuator. (**B**) Close–up from (**A**) with nerve suction electrodes (with silver wires), an intracellular electrodes and the 3 silicon probes (green) inserted into the spinal cord. (**C**) *Post–hoc* histological reconstruction of the location of three Berg64–probes. The probes had been painted with DiI prior to insertion leaving a blue fluorescent trace of each shank. The tissue is also immuno–stained for ChAT neurons (green) and for cells in general with DAPI (red). Inset illustration indicates lateral sections of slices 4, 5 and 6.

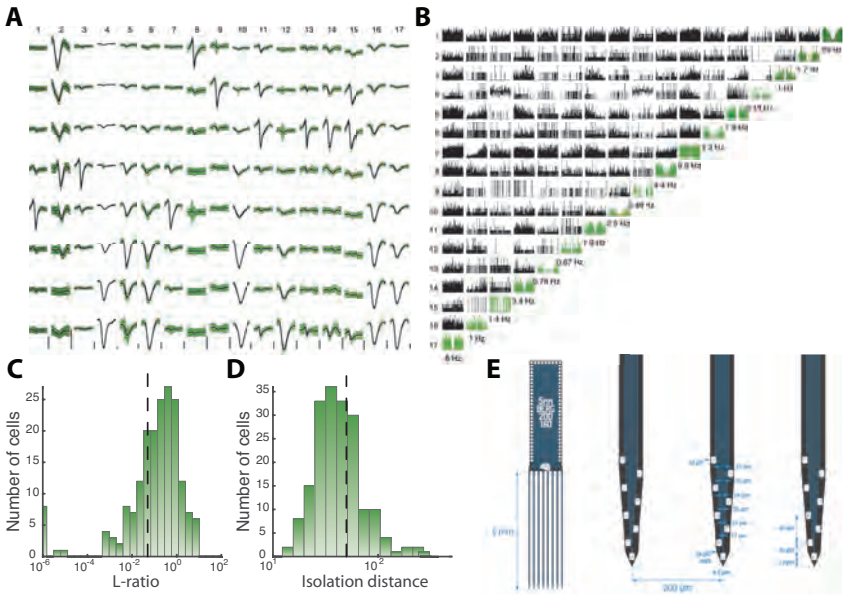

figure supplement 2: Sorted sample units, quality measures, probe layout and histology. (**A**) Waveforms of 17 units (columns) recorded with 8 electrodes (rows) from the same shank of a Berg64–probe. One standard deviation of the spike–shape variability is highlighted in green. vertical scale bar $100\mu V$. (**B**) Correlogram matrix for the same 17 units with the autocorrelograms in green. The qualitiy metrics of the spike sorting the *L-ratio* (**C**) and *Isolation distance* (**D**) for all units from the same session. (**E**) The Berg64–probe (Neuronexus inc) consists of 8 shanks with 8 leads on each shanks, located at the edge to cover most tissue. Dimensions are indicated.

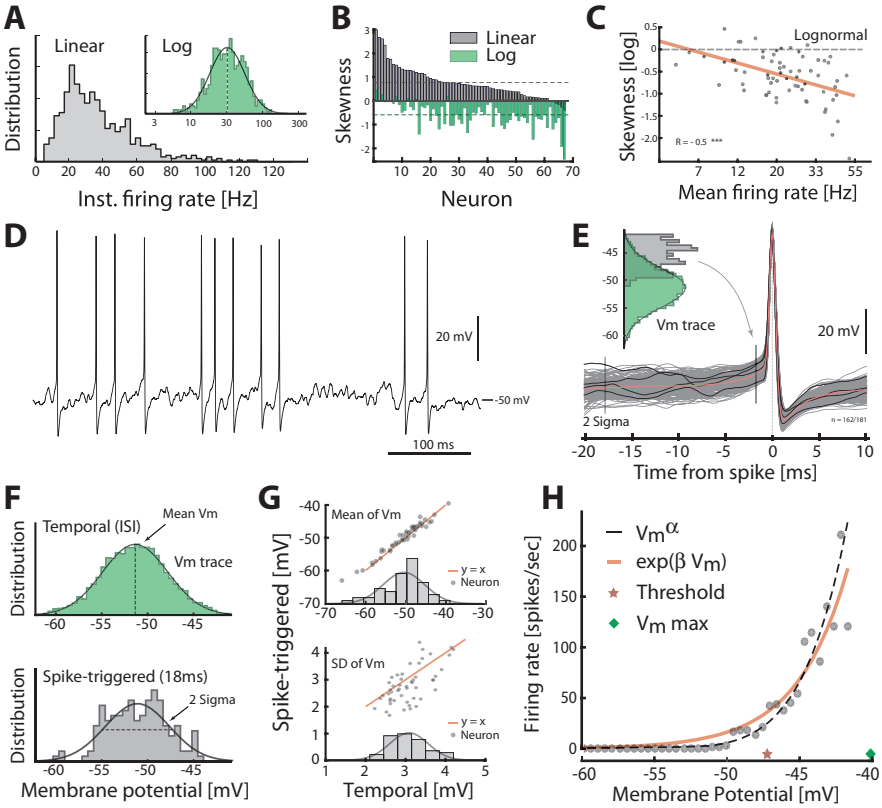

Figure 3: Spiking properties for serially acquired intracellular recorded neurons. (**A**) Distribution of instantaneous firing rates for a sample neuron is positively skewed on a linear axis and lognormal–like (green histogram, inset). Mean indicated by broken vertical line. (**B**) Sorted distribution skewness on linear (gray) and logarithmic axes (green) for each neuron in the population. (**C**) The log–skewness across neurons is negatively correlated ($R = -0.5$, $p < 0.001$) with mean firing rate indicating higher firing rates are found in the mean–driven regime and are less lognormally–distributed (broken line). (**D**) Sample cell spiking in the fluctuation–regime, and (**E**) its spike–triggered overlay to determine the V_m–distribution of trajectories prior to spike–onset (green histogram, 1.7 ms prior to peak) to compare with the total V_m–distribution (gray histogram). (**F**) V_m–distribution over time (spikes removed, top) and the spike–triggered V_m–distribution 18 ms prior to peak (left vertical line in **E**). (**G**) Mean temporal– against the spike–triggered–estimation (top) are closely related (orange unity–line) and have a near normal distribution of means (inset). For details, see Figure supplement 1 and 2. Similarly, the two estimates of SD are closely related (bottom). (H) The subthreshold IO–function is non-linear. Power-law and exponential are fitted to capture the curvature. For details, see Figure supplement 3.

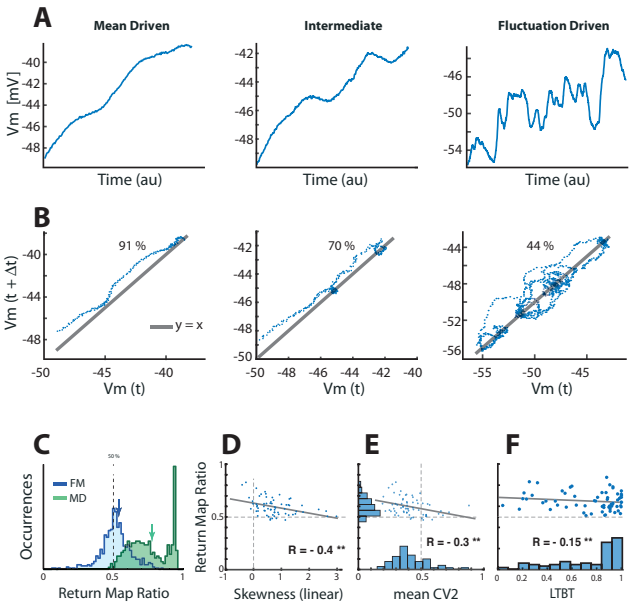

figure supplement 1: Quantifying the degree of fluctuations and selecting neurons in fluctuation–regime using the return map ratio metric. (**A**) The inter–spike V_m–trajectory of three sample neurons in mean–driven (left), intermediate (middle) and fluctuation–driven spiking regime (right). In the mean–driven regime the inter–spike trajectory moves directly from AHP resetting towards threshold, whereas in the fluctuation–driven regime the trajectory is convoluted and indirect (left). (**B**) The degree of convolution in the trajectory can be quantified using *return map*, i.e. plotting $V_m(t)$ versus $V_m(t + \Delta t)$, and quantifying the fraction of points above versus below the unity-line, referred to as the *return map ratio*. An even ratio close to 0.5 represents convolved V_m path (left), whereas a uneven ratio (close to 1) represent a direct path (right). (**C**) This return map ratio is calculated for all ISI shown for two sample neurons, one having distribution mean close to 0.5, i.e. a fluctuation–driven regime whereas the other have mean close to 0.8, i.e. in the mean–driven regime. Neurons having return map ratio below 0.7 was selected as being in the fluctuation–regime. The return map ratio of the population ($n = 68$) has a significant negative correlation with skewness of spike rate distribution (**D**) and spike irregularity (CV_2) (**E**) as well as the least time spent below threshold of V_m (**F**).

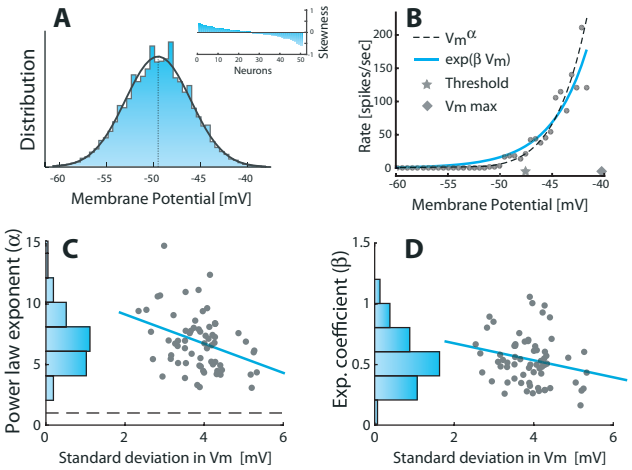

figure supplement 2: Properties of the subthreshold V_m–distribution and the spike–response curve. (**a**) A sample V_m–distribution in–between spikes is symmetric and near normal–distributed. Gaussian fit shown as black line. (**b**) The sorted skewness of all neurons in the fluctuation–regime, i.e. have return map ratio below 0.7. The skewness is clustered around and close to zero (Compare with Figure 3B). (**c**) The subthreshold spike response versus V_m for a sample neuron. A power–law (broken line) and an exponential (orange line) are fitted to capture the nonlinearity. (**d**) Power–law exponents (α) for different neurons are inversely correlated with the fluctuations in their V_m as quantified as the standard deviation of the inter–spike V_m ('sigma', Figure 3E, $R = -0.34$, $p < 0.01$). Linearity is indicated by horizontal broken line. (**e**) Exponential coefficient (β) for different neurons are also inversely correlated with the fluctuations in V_m though not significantly ($R = -0.22$, $p > 0.05$).

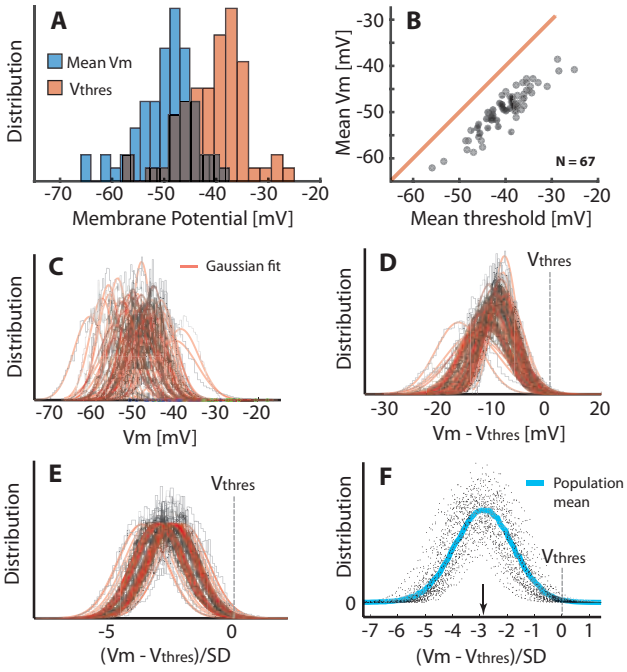

figure supplement 3: Population–distribution of V_m is Gaussian. (**a**) The mean V_m for the population of neurons is symmetrically near Gaussian–distributed (blue). The mean threshold for the same population is depolarized (red). (**b**) The mean thresholds correlate with the values of mean V_m and the thresholds are more depolarized as indicated by a rightward shift compared with the unity line (red). (**c**) Scatter plot of all the histograms of V_m with Gaussian fits (red). (**d**) Histogram of the V_m distributions with the individual mean thresholds (V_{thres}) subtracted (broken line indicates the relative location of V_{thres}). The V_m distributions that have their mean far from threshold also have a larger SD. (**e**) Normalizing each distribution with the sandard deviation (σ) to assess the normalized distance in terms of the size of fluctuations, i.e. $(V_m - V_{thres})/\sigma$. (**f**) Scatter plot of all the distributions of $(V_m - V_{thres})/\sigma$, has a near Gaussian distribution as indicated with the sliding population mean (blue). The mean distance to threshold is approximately 3σ (arrow).

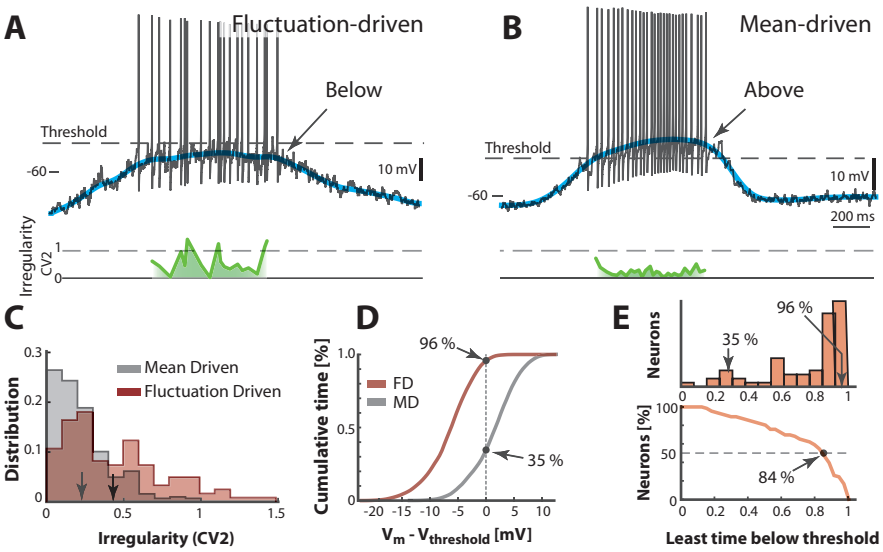

Figure 4: Time spent below threshold depends on regime. (**A**) Sample neuron, where the mean V_m (blue line) is below initial threshold (broken line), the spikes are irregular ($CV_2 \approx 0.5$–1, green line) and driven by fluctuations (arrow). (**B**) Second sample cell with mean–driven spiking, where the mean V_m is above threshold during the motor cycle (arrow). The spiking is more regular, i.e. low CV_2 (green line). (**C**) Distribution shows the mean–driven neuron (gray) has lower CV_2 than the fluctuation–driven neuron (brown). Means indicated. (**D**) Cumulative time of V_m shows the fluctuation–driven neuron (FD) spends more time below threshold (96%) than the mean–driven (MD, 35%) between spikes. (**E**) Top: Time below threshold for population of neurons (cells from A–D indicated). Bottom: Compound time spent below threshold versus a given fraction of neurons (reverse cumulative distribution function). Half of the neurons (broken line) spend at least 84% of the time in fluctuation–regime, i.e. have V_m below threshold.

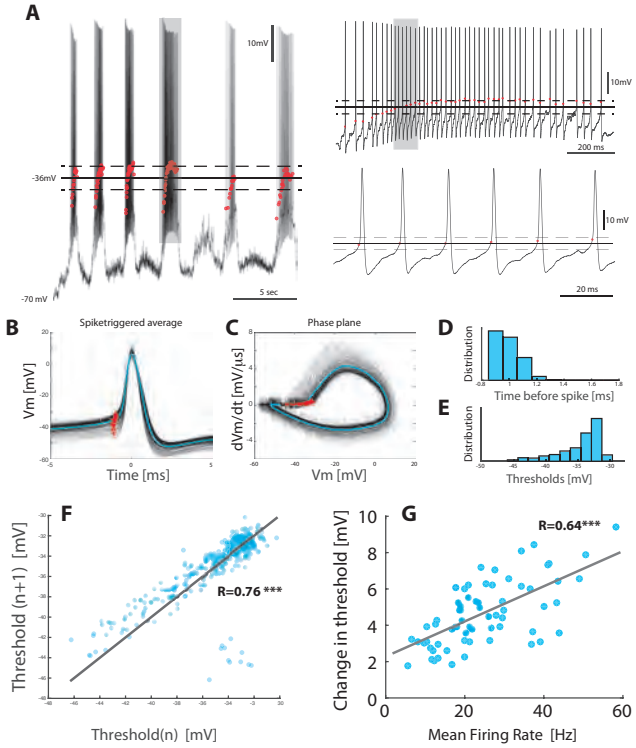

figure supplement 1: Threshold depolarizes with increase in spike rate. (**A**) Sample recording with the threshold (red dots) for each spike (left). Mean threshold (solid line) ± SD (broken lines). Right top: the selected cycle from trace in left (fourth cycle indicated by gray horizontal bar at top). Right bottom: Selected region on shorter timescale (gray rectangle from top trace). (**B**) Spike–triggered overlay with the thresholds indicated (red dots). (**C**) Detection of threshold via method by Sekerli *et al.* [2004]: Threshold is found at the maximum of the second derivative of the trajectory in phase plane plot of V_m versus dV_m/dt (red dots). (**D**) Distribution of threshold location prior to spike peak. (**E**) Distribution of threshold values in V_m. (**F**) A given threshold value (threshold n) has strong correlation with the neighboring threshold value (threshold $n+1$). (**G**) The change in threshold, $V_{thresh} - V_{thres,Q5}$, where $V_{thres,Q5}$ is the threshold at the 5% quintile and V_{thresh} is the threshold for individual spikes.

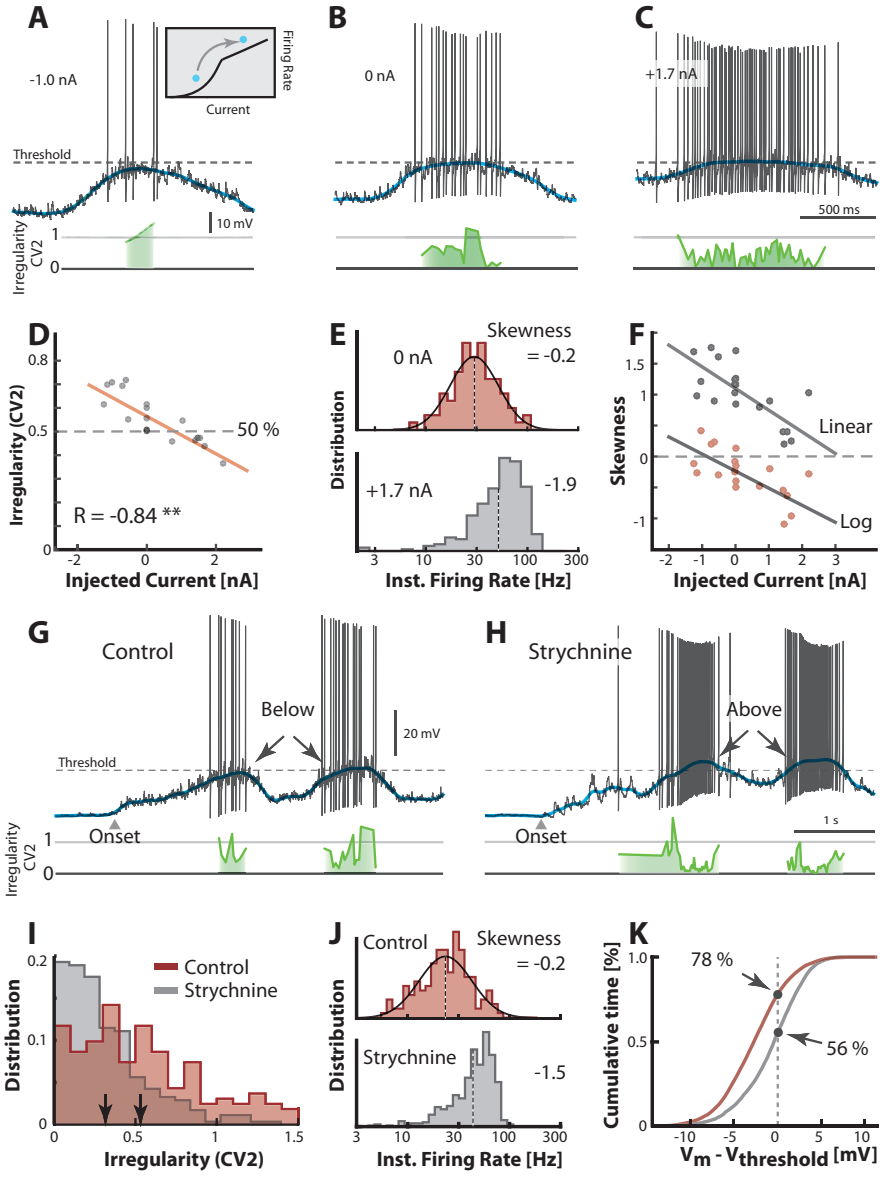

Figure 5: Transition between regimes induced by increasing input. (**A**) Sample neuron V_m during the motor cycle with negative injected current (-1.0 nA). Negative current hyperpolarizes mean V_m (blue) and increases irregularity ($CV_2 \approx 1$, green line) compared with control condition (**B**). (**C**) Positive current injection (1.7nA) has the opposite effect: Depolarization, more regular spiking and higher firing rate. (**D**) Means of CV_2 over multiple current injections has negative correlation. (**E**) Firing rate is lognormally distributed (control, top) and negatively skewed when injecting current (bottom, skewness = -1.9) consistent with transition from fluctuation– to mean–driven spiking. (**F**) Skewness is negatively correlated with injected current. Linear skewness top gray points ($R = -0.73$, $p < 0.001$) and log-skewness bottom red points ($R = -0.70$, $p < 0.001$). (**G**) Sample cell in control condition and after reduction of inhibition with local strychnine (**H**). (**I**) Irregularity (CV_2) was smaller after application of strychnine (arrows indicate mean). (**J**) Rate distribution is symmetric on log–scale (top, skewness =-0.2) and negatively skewed when inhibition is blocked (bottom, skewness=-1.5). (**K**) Cumulative time spent below threshold is higher, i.e. more hyperpolarized, in the control condition than after strychnine (compare 78% with 56%).

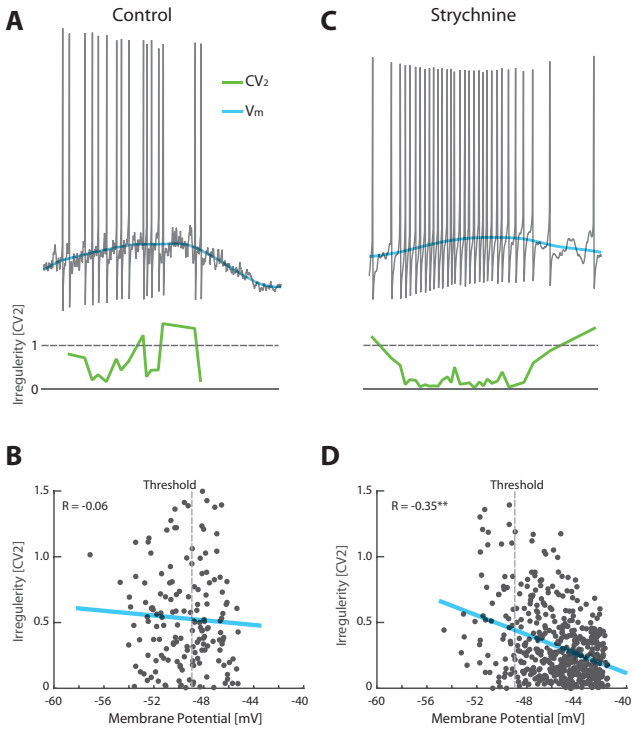

figure supplement 1: Unbalancing E/I induces an anti–correlation between irregularity and depolarization. (**A**) Sample cell with mean membrane potential (blue) and the irregularity of the spike (CV_2, green) in the control condition. (**B**) The spiking is in the fluctuation–driven regime, which is manifested as a lack of significant correlation between irregularity for each pair of ISIs (CV_2) and the mean V_m of the intervals ($R = -0.06$, $p = 0.48$). (**C**) Spiking of same cell as in (**A**) after elimination of glycinergic inhibition by local application of strychnine. (**D**) The removal of inhibition puts the spiking into the mean–driven regime, which is manifested as a significant negative correlation between irregularity of the spiking and the membrane depolarization ($R = -0.35$, $p \ll 0.0001$).

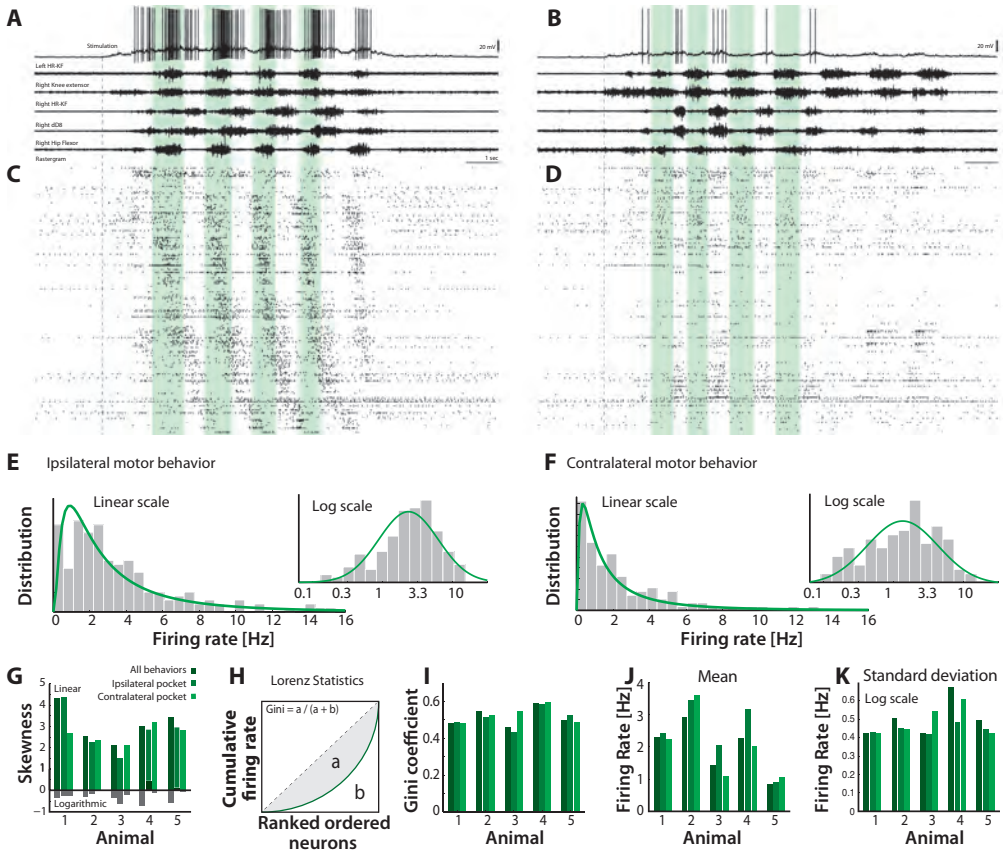

Figure 6: Skewed neuronal participation across behaviors. (**A-B**) Two distinct motor behaviors: Ipsilateral pocket scratch (left panel) and contralateral pocket scratch (right panel) shown by intracellular recordings (top) and motor nerve activities. (**C-D**) Rastergrams showing the unit activities during ipsilateral pocket scratch (**C**) and contralateral pocket scratch (**D**). Green areas mark the hip flexor phase. (**E-F**) firing rate distribution for the behaviors on linear and a semi-log plot (insets), indicate lognormal participation. Lognormal functions are fitted (solid green lines). (**G**) Skewness on logarithmic (green bars) and linear scale (gray bars) is preserved across animals. (**H**) The inequal neuronal participation is calculated using Lorenz curve and gini coefficient. (**I**) Gini–coefficients cluster around 0.5 across behaviors and animals. (**J**) Mean and standard deviation (**K**) of the distribution of firing rates across behaviors and animals.

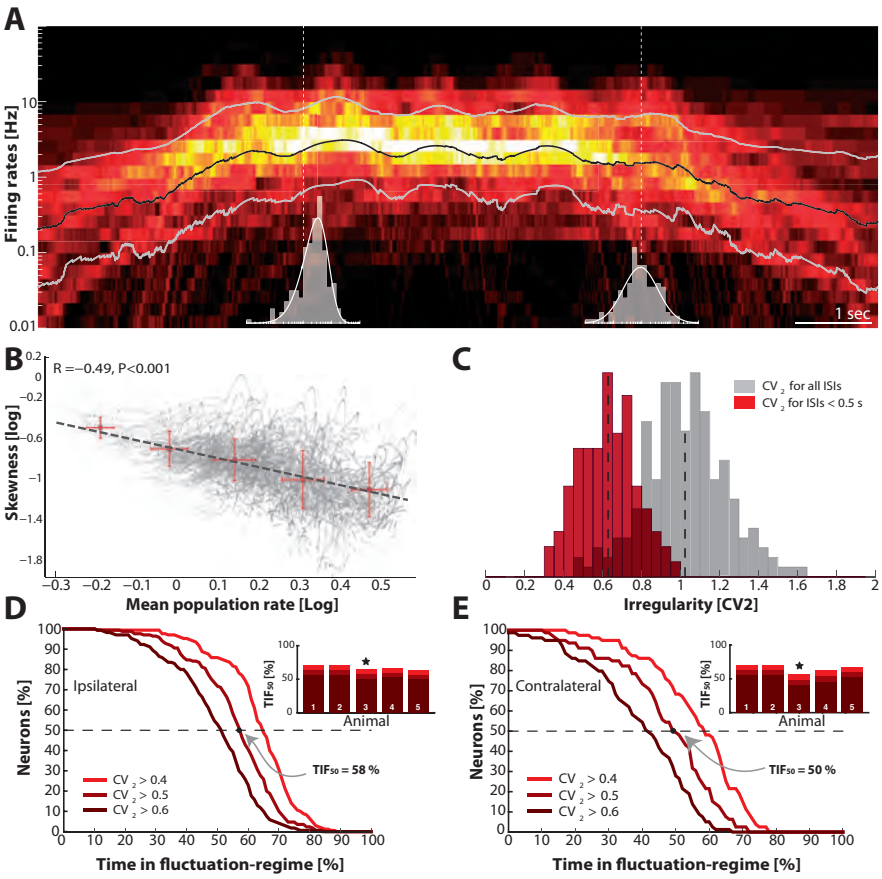

Figure 7: Skewness and irregularity across the neuronal population gauge occupation in both regimes across time. (**A**) Heat map of the distribution of firing rates across the population on log–scale (y–axis) as a function of time (x–axis). Lognormal mean ± SD are indicated as black and grey lines, respectively. Distribution is indicated (gray histograms) at two different time points (broken vertical lines). (**B**) Lognormal mean population firing rate versus log–skewness are negatively correlated, indicating more neurons move into mean–regime as the population rate increases. (**C**) Distribution of irregularity (mean CV_2) across population for all ISIs (gray) and when excluding of inter–burst intervals (red). (**D**) Reverse cumulative distribution of neurons, which spend a given amount of time in fluctuation–regime ($i_{crit} = 0.4, 0.5$ and 0.6) normalized to 100%. The least time spent in fluctuation–regime by half of the neurons (TIF_{50}) is given by the intercept with the broken horizontal line and distribution (indicated by arrow). For this sample animal and behavior $TIF_{50} = 56\%$. Inset: Values across animals, sample animal indicated ($\star$). (**E**) The TIF_{50}–values across animals in both behaviors as indicated by similarity in values are remarkably conserved.

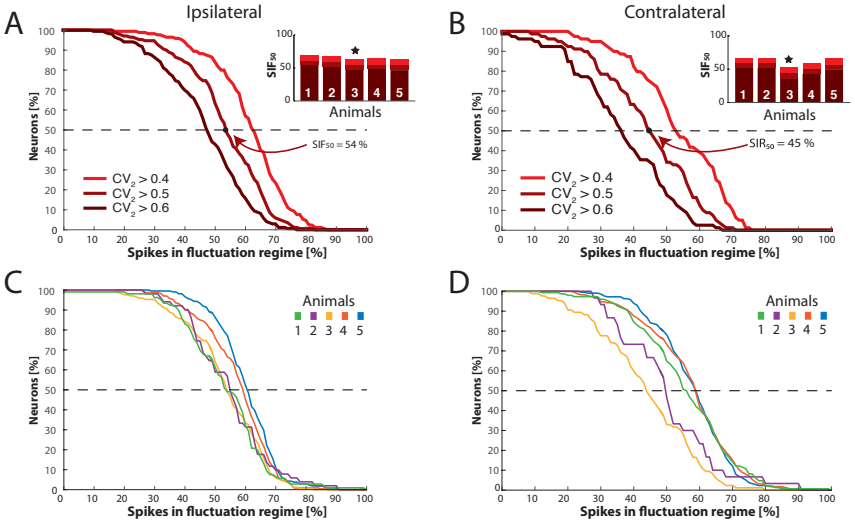

figure supplement 1: Distribution of neurons having fluctuation driven spikes and SIF_{50} values. (**A**) Reverse cumulative distribution of neurons (y–axis) having a given number of spikes driven by fluctuations (x–axis) for ipsilateral scratching for a sample animal and three values of i_{crit} (0.4, 0.5, and 0.6). The minimal fraction of spikes driven by fluctuation in half of the neuronal population, SIF_{50}, shown in inset. Sample animal indicated ($\star$). (**B**) Same as (**A**) but for contralateral scratching. (**C**) The reverse cumulative distributions similar to (**A**) for all five animals and for $i_{crit} = 0.5$ for ipsilateral scratching and for contralateral scratching (**D**).